Available online at www.sciencedirect.com

ScienceDirect

International Journal of Solids and Structures 43 (2006) 7891–7918

INTERNATIONAL JOURNAL OF SOLIDS and STRUCTURES

www.elsevier.com/locate/ijsolstr

Design optimization of truss-cored sandwiches with homogenization

T. Liu [a], Z.C. Deng [a,b], T.J. Lu [c,d,*]

[a] *Department of Engineering Mechanics, Northwestern Polytechnical University, Xi'an 710072, PR China*
[b] *State Key Laboratory of Structural Analysis of Industrial Equipment, Dalian University of Technology, Dalian 116024, PR China*
[c] *School of Aerospace, Xi'an Jiaotong University, Xi'an 710049, PR China*
[d] *Department of Engineering, University of Cambridge, Cambridge CB2 1PZ, UK*

Received 5 January 2006; received in revised form 3 April 2006
Available online 22 April 2006

Abstract

Lightweight metallic sandwich plates comprising periodic truss cores and solid facesheets are optimally designed against minimum weights. Constitutive models of the truss core are developed using homogenization techniques which, together with effective single-layer sandwich approaches, form the basis of a two-dimensional (2D) single-layer sandwich model. The 2D model is employed to simulate the mechanical behaviors of truss-cored sandwich panels having a variety of core topologies. The types of loading considered include bending, transverse shear and in-plane compression. The validities of the 2D model predictions are checked against direct FE simulations on three-dimensional (3D) truss core sandwich structures. Optimizations using the 2D sandwich model are subsequently performed to determine the minimum weights of truss-cored sandwiches subjected to various failure constraints: overall and local buckling, yielding and facesheet wrinkling. The performances of the optimized truss core sandwiches with 4-rod unit cell and solid truss members and pyramidal unit cell with hollow truss members are compared with benchmark lightweight structures such as honeycomb-cored sandwiches, tetrahedral core sandwiches and hat-stiffened single layer plates.

Keywords: Truss lattice materials; Homogenization; Finite element method; Sandwich plate; Design optimization; Buckling; Plastic yielding

1. Introduction

Highly porous, periodic metallic lattice materials at length scales of 0.1–10 mm have emerged recently with novel manufacturing techniques (Gustafsson, 2000; Evan et al., 2001; Wadley et al., 2003). Typical topologies of lattice materials that have been studied both experimentally and theoretically are depicted in Fig. 1 (Kooistra et al., 2004). These lattice materials are basically sandwich systems consisting of a three-dimensional

* Corresponding author. Address: Department of Engineering, University of Cambridge, Trumpington Street, Cambridge CB2 1PZ, United Kingdom. Tel.: +86 29 82665600/+44 1223 766316; fax: +86 29 83234781/+44 1223 332662.
E-mail address: tjlu@mail.xjtu.edu.cn (T.J. Lu).

0020-7683/$ - see front matter
doi:10.1016/j.ijsolstr.2006.04.010

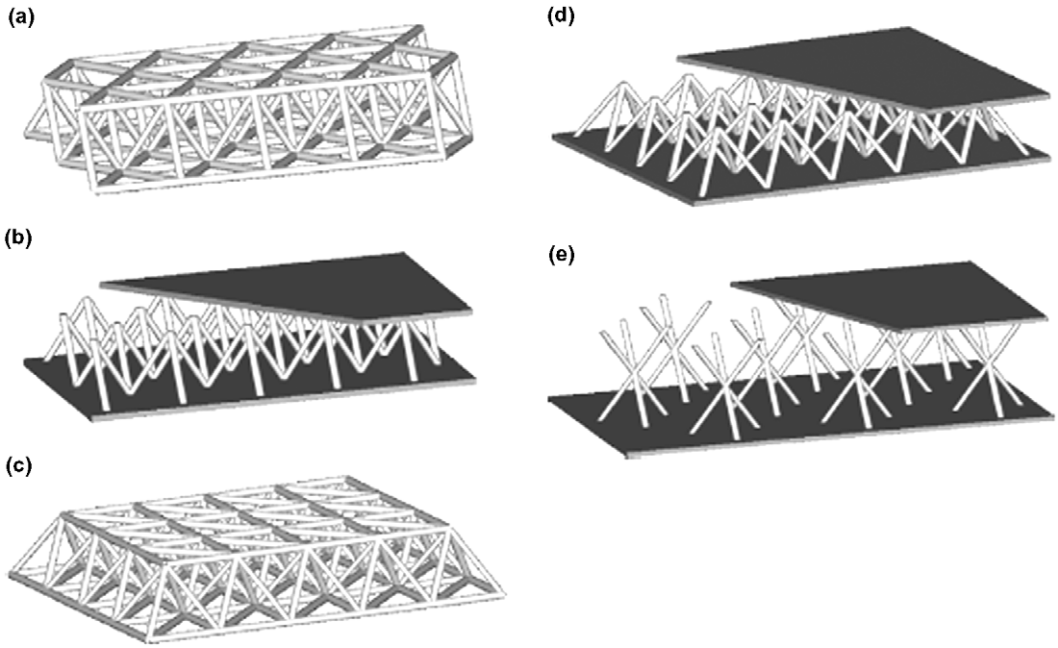

Fig. 1. Typical lattice truss topologies: (a) octet truss, (b) tetrahedral lattice truss, (c) lattice block, (d) pyramidal lattice truss and (e) 3D kagome.

(3D) network of fully triangulated solid (or hollow) rods. Potential applications include blast resistant structures (Hutchinson and Xue, 2005), multifunctional materials (e.g., simultaneously load bearing and active cooling; see Kim et al., 2004; Tian et al., 2004), and replacement for the structurally efficient but expensive honeycombs (Evan et al., 2001; Wicks and Hutchinson, 2001, 2003; Wallach and Gibson, 2001).

The minimum weight design of sandwich panels comprised of tetrahedral truss cores faced with either triangulated or solid sheets was first studied by Wicks and Hutchinson (2001, 2003). Optimal designs for both compression panels and panels subjected to combined loads of bending and transverse shear were obtained. Compared with hat-stiffened plates that are generally regarded as one of the most weight efficient constructions for compression panels (Budiansky, 1999; Tian and Lu, 2005), it was established that the optimized truss core sandwich plates offer greater weight savings and design advantages. Compared with sandwiches with hexagonal honeycomb cores, which have long been considered as the most structurally efficient systems under bending and transverse shear loads, the optimized truss core sandwich plates are found to be equally effective (Wicks and Hutchinson, 2001, 2003).

Wallach and Gibson (2001) used the unit cell approach to calculate the elastic moduli, uniaxial compressive strength and shear strength of sandwich structures having pyramidal truss cores; the predictions agree well with experimental measurements. Deshpande and Fleck (2001) studied the minimum weight of sandwich beams with tetrahedral truss cores subjected to 3-point bending. Collapse equations for face yielding, face wrinkling and core shear of the sandwich were established, and a graphical method based on collapse mechanism map was used for optimization. It was found that the resulting minimum weight design is about 30% greater than the global minimum obtained by Wicks and Hutchinson (2001). Liu and Lu (2004) explored the multi-objective and multi-loading design optimization of sandwich plates comprised of either tetrahedral or plagihedral pyramidal truss cores and solid facesheets. The plagihedral pyramidal unit cell was first introduced for lattice materials in this study.

Previous researches on truss core sandwiches focused mainly on several standard cell topologies: tetrahedral (Wicks and Hutchinson, 2001; Deshpande and Fleck, 2001), pyramidal (Wallach and Gibson, 2001), plagihedral pyramidal (Liu and Lu, 2004), Kagomé (Hyun et al., 2003), and octet truss (Deshpande et al., 2001). The possibility of achieving more competitive yet relatively simple unit cell topologies for truss core sandwich

constructions is examined in the present study. To this end, a computationally efficient model is employed: the truss core is firstly homogenized into a homogeneous medium, which is subsequently used to construct an effective single-layer sandwich model (Allen, 1969; Hohe and Librescu, 2004; Kollar and Springer, 2003). The predictions of the model are validated against FE results obtained directly with 3D truss-cored sandwich plates. For comparison, it is noticed that the simplified computational method used by Wicks and Hutchinson (2001) is most suitable for optimization of simple truss core configurations and simple structures (e.g., a wide sandwich plate with tetrahedral cores under 3-point bending) whereas the discrete 3D computational model of Liu and Lu (2004) can be too complicated and time consuming for optimization calculations.

2. Formulation of truss core homogenization

Straalen (2000) presented a comprehensive overview of theoretical developments for sandwich panels, which can be classified as the classical theories, the superposition approaches and the higher-order theories. Two-dimensional finite element computational models for sandwich panels and shells were critically reviewed by Noor et al. (1996), and can be classified as the global approximation models, discrete three layer models and the predicator–corrector approaches. Computationally efficient models for sandwiches are typically based on the equivalent replacement of the core with a homogeneous continuum. The reliability of continuum modeling is critically dependent on the accuracy of the effective core properties. For frequently used 2D cellular materials such as honeycombs, the homogenization techniques (e.g., the strain energy based approaches and the mathematical homogenization based on a two-scale expansion of the displacement field) were reviewed by Hohe and Becker (2002). Ziegler et al. (2004) proposed a continuum plate model for lattice block materials by using the FE formulation for a thick plate. The agreement between predictions obtained with the continuum plate model and those with the discrete FE model is in general good for bending, in-plane behavior and dynamic modal analysis. However, for the coupled behavior of the sandwich under combined bending and in-plane forces, the agreement is not as good.

The key problem facing truss core homogenization is the establishment of a suitable mechanical model for the 3D network of rods within the core. For octet trusses, due to the large aspect ratio of rod length to rod radius, the rods may be assumed to be pin-jointed at the nodes (Deshpande et al., 2001). Consequently, the contribution to the overall stiffness from bending of the rods can be neglected, in comparison with the contribution by rod stretching/compression. For octet truss materials or octet truss sandwiches with triangulated facesheets, this assumption has been verified by FE calculations (Deshpande and Fleck, 2001). For truss core sandwiches with solid facesheets, however, the constraints imposed on the rod deformation may no longer be negligible. Consequently, in the present study, the rods in the truss core are modeled using Euler–Bernoulli beams, with clamped support at both ends. Furthermore, the following assumptions are made:

(1) There is no intersection amongst truss members within the truss core, which implies that the present approach is applicable to tetrahedral and pyramidal cores but not to Kagom$\doteq$ cores (Fig. 1).
(2) The displacements of truss members are small, i.e., small strains and small rotations are in place.
(3) The truss members are solid/hollow cylinders with circular/tube cross-sections, and are made of the same base material.
(4) The influence of edge effect is negligible.
(5) The facesheets are rigid in comparison with the relatively compliant truss core.
(6) No truss core members are present in the facesheet planes.

2.1. Homogenization

A truss material may be analyzed at two different scales: (a) at the macroscale, it is treated as a homogeneous solid; (b) at the microscopic scale, discrete truss structures are considered. The derivation of the micro–macro relations for a heterogeneous medium relies on the analysis of its representative volume element (RVE, or unit cell in this paper). For periodic media such as the lattice structures, the smallest periodic unit is commonly taken as the unit cell.

Following the modern notations of continuum mechanics, at the microscale, let $\boldsymbol{\sigma}$ denote the stress tensor and $\boldsymbol{\varepsilon}$ denote the strain tensor and, at the macroscale, let $\boldsymbol{\Sigma}$ denote the macroscopic stress tensor and $\mathbf{E}$ denote the macroscopic strain tensor. Here and throughout the rest of this paper, tensorial variables are represented by bold symbols. The homogenized micro–macro relationship can then be described as

$$\mathbf{E} = \langle \boldsymbol{\varepsilon} \rangle_{\Omega} \equiv \frac{1}{\Omega} \int_{\Omega} \boldsymbol{\varepsilon} \, \mathrm{d}\Omega, \tag{1}$$

$$\boldsymbol{\Sigma} = \langle \boldsymbol{\sigma} \rangle_{\Omega} \equiv \frac{1}{\Omega} \int_{\Omega} \boldsymbol{\sigma} \, \mathrm{d}\Omega, \tag{2}$$

where Ω represents the current volume of unit cell and $\langle \bullet \rangle_{\Omega}$ denotes volume averaging. For statically admissible stress field $\boldsymbol{\sigma}$ and kinematically admissible strain field $\boldsymbol{\varepsilon}$, the macrohomogeneity equality of Hill (1963) dictates that:

$$\boldsymbol{\Sigma} \bullet \mathbf{E} = \langle \boldsymbol{\sigma} \bullet \boldsymbol{\varepsilon} \rangle_{\Omega} = \frac{1}{\Omega} \int_{\Omega} \boldsymbol{\sigma} \bullet \boldsymbol{\varepsilon} \, \mathrm{d}\Omega, \tag{3}$$

where $\boldsymbol{\Sigma} \bullet \mathbf{E}\Omega$ is the macroscopic strain energy density and $\int_{\Omega} \boldsymbol{\sigma} \bullet \boldsymbol{\varepsilon} \, \mathrm{d}\Omega$ is the total strain energy density of the admissible microscopic fields. Hill's relation implies that the volume averaged strain energy density of an inhomogeneous material can be obtained by multiplying the separate volume averages of microscopic stresses and strains.

2.2. Small strain kinematics

Mohr (2005) studied the mechanical behaviors of ideal truss lattice materials controlled by the so-called direct action mechanism at the microscale. A general micromechanics-based finite-strain constitutive model was presented, but only the stretching and compression of individual truss members were considered. In this paper, we go further and present the homogenized results using a beam model. It is assumed that the rods in unit cell are embedded in an infinitely soft matrix (Suquet, 1987). For small strain deformations, the deformation of the unit cell is also small, i.e., the deformation of the facesheets has negligible influence on the geometry of the unit cell.

Consider the deformation from time 0 to T of a unit cell comprising a single rod, as schematically shown in Fig. 2. The displacement of a material point initially located at position $\mathbf{X}$ in the reference configuration to position $\mathbf{x}$ in the current configuration is formally described by the point-to-point mapping $\mathbf{x} = \boldsymbol{\varphi}(\mathbf{X}, t)$, where

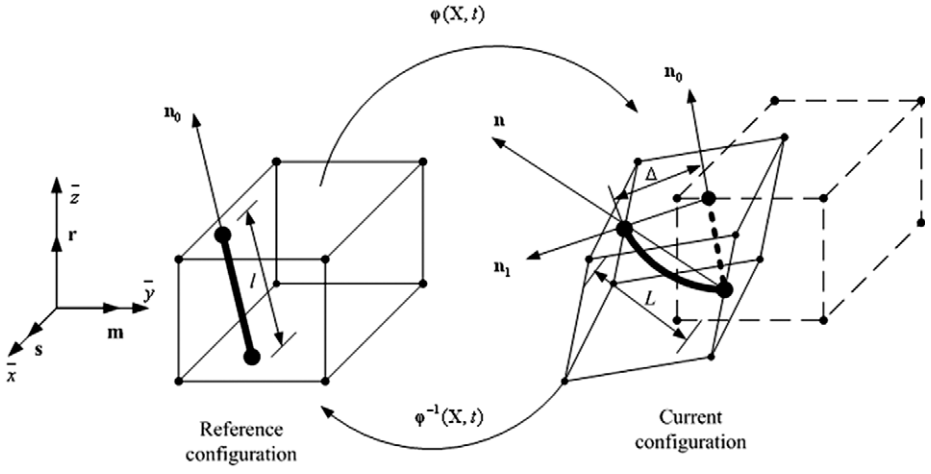

Fig. 2. Kinematics of a unit cell (RVE) comprising a single rod embedded in an infinite soft matrix.

$t \in [0, T]$ represents time. The deformation gradient $\mathbf{F} = \mathbf{F}(\mathbf{X})$ is defined by the gradient of this transformation as

$$\mathbf{F} = \nabla\boldsymbol{\varphi}. \tag{4}$$

Therefore, the linear transformation can be formulated as

$$\mathrm{d}\mathbf{x} = \mathbf{F}\,\mathrm{d}\mathbf{X}, \quad \det\mathbf{F} > 0. \tag{5}$$

The displacement field $\mathbf{u}$ can be defined as

$$\mathbf{u}(\mathbf{X}, t) = \boldsymbol{\varphi}(\mathbf{X}, t) - \mathbf{X}. \tag{6}$$

It follows from (4) that the displacement gradient is given by

$$\nabla\mathbf{u} = \mathbf{F} - \mathbf{I}, \quad \nabla u_{ij} \ll 0 \ \ (i, j = 1, 2, 3), \tag{7}$$

where small displacements have been assumed.

The homogeneity of the displacement field implies that the deformation gradient is uniform within the unit cell. The macroscopic Green strain tensor $\mathbf{E}$ can be defined with respect to the reference configuration, as (Lai et al., 1993)

$$\mathbf{E} = \tfrac{1}{2}(\mathbf{C} - \mathbf{I}), \tag{8}$$

where $\mathbf{C}$ is the Cauchy–Green tensor:

$$\mathbf{C} = \mathbf{F}^{\mathrm{T}}\mathbf{F}, \tag{9}$$

and the superscript 'T' denotes transposition. Using Eq. (7), we have

$$\mathbf{E} = \tfrac{1}{2}\Big[(\nabla\mathbf{u} + \mathbf{I})^{\mathrm{T}}(\nabla\mathbf{u} + \mathbf{I}) - \mathbf{I}\Big] \approx \nabla\mathbf{u} = \operatorname{sym}\nabla\mathbf{u} = \tfrac{1}{2}(\nabla\mathbf{u}^{\mathrm{T}} + \nabla\mathbf{u}). \tag{10}$$

As shown in Fig. 2, a truss member initially aligned with the unit vector $\mathbf{n}_0$ is rotated into the current direction $\mathbf{n}$. For small deformations, the distance L between the ends of the rod is approximately equal to the length of the rod after deformation (Fig. 2), i.e.,

$$L\mathbf{n} = \mathbf{F}l\mathbf{n}_0, \tag{11}$$

$$\boldsymbol{\Delta} = \Delta\mathbf{n}_1 = L\mathbf{n} - l\mathbf{n}_0 = (\mathbf{F} - \mathbf{I})l\mathbf{n}_0, \tag{12}$$

where l is the initial length of the rod and $\boldsymbol{\Delta}$ is the displacement of the end point of the rod (Fig. 2). From Eqs. (7) and (10), we have:

$$\boldsymbol{\Delta} = l\mathbf{E}\mathbf{n}_0, \tag{13}$$

where

$$\mathbf{E} = \begin{bmatrix} E_{11} & E_{12} & E_{13} \\ & E_{22} & E_{23} \\ \text{sym.} & & E_{33} \end{bmatrix}, \tag{14}$$

$$\mathbf{n}_0 = (n_{01}, n_{02}, n_{03})^{\mathrm{T}}. \tag{15}$$

With $\mathbf{m}$, $\mathbf{s}$, $\mathbf{r}$ denoting separately the unit vectors aligned with the axes of coordinates $\bar{x}$, $\bar{y}$, $\bar{z}$ in the reference configuration (Fig. 2) and Δ_1, Δ_2, Δ_2 denoting the projections of $\boldsymbol{\Delta}$, we have:

$$\boldsymbol{\Delta} = \Delta\mathbf{n}_1 = (\Delta_1\mathbf{m}, \Delta_2\mathbf{s}, \Delta_3\mathbf{r})^{\mathrm{T}}. \tag{16}$$

2.3. Homogenized macroscopic equivalent properties

For a unit cell containing N Euler–Bernoulli beam members, the strain energy density may be defined as

$$U^* = \frac{1}{\Omega}\sum_{i=1}^{N}\frac{1}{2}\tilde{\mathbf{u}}^{(i)\mathrm{T}}\widetilde{\mathbf{K}}^{(i)}\tilde{\mathbf{u}}^{(i)}, \tag{17}$$

where $\tilde{\mathbf{u}}^{(i)}$ is the nodal displacement vector for the ith beam characterized by the end nodes ζ and τ, as shown Fig. 3:

$$\tilde{\mathbf{u}}^{(i)} = \left[w_\zeta, v_\zeta, \psi_\zeta, \theta_{\zeta x}, \theta_{\zeta y}, \theta_{\zeta z}, w_\tau, v_\tau, \psi_\tau, \theta_{\tau x}, \theta_{\tau y}, \theta_{\tau z}\right]^{(i)\mathrm{T}}. \tag{18}$$

From Fig. 2 as well as Eq. (16), one can write:

$$\tilde{\mathbf{u}}^{(i)} = [\Delta_1, \Delta_2, \Delta_3, 0, 0, 0, 0, 0, 0, 0, 0, 0]^{(i)\mathrm{T}}. \tag{19}$$

In Eq. (17), $\widetilde{\mathbf{K}}^{(i)}$ is the global stiffness matrix that satisfies the transformation between local and global coordinates, as shown in Fig. 3:

$$\widetilde{\mathbf{K}}^{(i)} = \mathbf{T}^{\mathrm{T}}\widetilde{\mathbf{K}}^{\mathrm{e}(i)}\mathbf{T}, \tag{20}$$

$$\widetilde{\mathbf{K}}^{(i)} = \begin{bmatrix} k_{11} & k_{12} & k_{13} & k_{14} & k_{15} & k_{16} & \cdots \\ & k_{22} & k_{23} & k_{24} & k_{25} & k_{26} & \cdots \\ & & k_{33} & k_{34} & k_{35} & k_{36} & \cdots \\ & & & k_{44} & k_{45} & k_{46} & \cdots \\ & \text{sym.} & & & k_{55} & k_{56} & \cdots \\ & & & & & k_{66} & \cdots \\ & & & & & & \cdots \end{bmatrix}^{(i)}, \tag{21}$$

where $\mathbf{T}$ is the transformation matrix and $\widetilde{\mathbf{K}}^{\mathrm{e}(i)}$ is the elementary stiffness matrix of the ith beam. For Euler–Bernoulli beams:

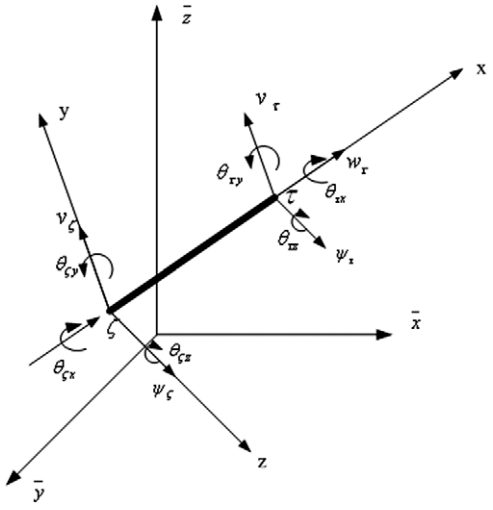

Fig. 3. Displacements and rotations at nodes ζ and τ of ith beam member in local coordinates (x, y, z). Transformation from local coordinates to global coordinates $(\bar{x}, \bar{y}, \bar{z})$ is defined by transformation matrix $\mathbf{T}$.

$$\widetilde{\mathbf{K}}^{\mathrm{e}(i)} = \begin{bmatrix} \widetilde{\mathbf{K}}_1 & \widetilde{\mathbf{K}}_2 \\ \text{sym.} & \widetilde{\mathbf{K}}_3 \end{bmatrix}^{\mathrm{e}(i)}, \tag{22}$$

$$\widetilde{\mathbf{K}}_1 = \begin{bmatrix} \frac{EA}{l} & 0 & 0 & 0 & 0 & 0 \\ 0 & \frac{12EI_z}{l^3} & 0 & 0 & 0 & \frac{6EI_z}{l^2} \\ 0 & 0 & \frac{12EI_y}{l^3} & 0 & \frac{-6EI_y}{l^2} & 0 \\ 0 & 0 & 0 & \frac{GI_x}{l} & 0 & 0 \\ 0 & 0 & \frac{-6EI_y}{l^2} & 0 & \frac{4EI_y}{l} & 0 \\ 0 & \frac{6EI_z}{l^2} & 0 & 0 & 0 & \frac{4EI_z}{l} \end{bmatrix}, \tag{23}$$

$$\widetilde{\mathbf{K}}_2 = \begin{bmatrix} -\frac{EA}{l} & 0 & 0 & 0 & 0 & 0 \\ 0 & -\frac{12EI_z}{l^3} & 0 & 0 & 0 & \frac{6EI_z}{l^2} \\ 0 & 0 & -\frac{12EI_y}{l^3} & 0 & \frac{-6EI_y}{l^2} & 0 \\ 0 & 0 & 0 & -\frac{GI_x}{l} & 0 & 0 \\ 0 & 0 & \frac{6EI_y}{l^2} & 0 & \frac{2EI_y}{l} & 0 \\ 0 & -\frac{6EI_z}{l^2} & 0 & 0 & 0 & \frac{2EI_z}{l} \end{bmatrix}, \tag{24}$$

$$\widetilde{\mathbf{K}}_3 = \begin{bmatrix} \frac{EA}{l} & 0 & 0 & 0 & 0 & 0 \\ 0 & \frac{12EI_z}{l^3} & 0 & 0 & 0 & -\frac{6EI_z}{l^2} \\ 0 & 0 & \frac{12EI_y}{l^3} & 0 & \frac{6EI_y}{l^2} & 0 \\ 0 & 0 & 0 & \frac{GI_x}{l} & 0 & 0 \\ 0 & 0 & \frac{6EI_y}{l^2} & 0 & \frac{4EI_y}{l} & 0 \\ 0 & -\frac{6EI_z}{l^2} & 0 & 0 & 0 & \frac{4EI_z}{l} \end{bmatrix}, \tag{25}$$

where E and G are the Young's and shear moduli of the isotropic base material, l is the length of the ith beam member having cross-sectional area A, and I_x, I_y, I_z are the moments of inertia of the ith beam.

Let the macroscopic strain vector of the unit cell be defined as

$$\boldsymbol{\Xi} = [\Xi_{11}, \Xi_{22}, \Xi_{33}, \Xi_{23}, \Xi_{13}, \Xi_{12}]^{\mathrm{T}} = [E_{11}, E_{22}, E_{33}, 2E_{23}, 2E_{13}, 2E_{12}]^{\mathrm{T}}. \tag{26}$$

Then the effective stiffness of the unit cell can be calculated as

$$C^{\mathrm{H}}_{ijkl} = \frac{\partial^2 U^*}{\partial \Xi_{ij} \partial \Xi_{kl}}, \tag{27}$$

where the superscript 'H' denotes the homogenized effective stiffness. In compact form, we have:

$$C_{11}^{\mathrm{H}} = \frac{1}{\Omega}\sum_{i=1}^{N} l^{(i)2} n_{01}^{(i)2} k_{11}^{(i)}, \qquad C_{12}^{\mathrm{H}} = \frac{1}{\Omega}\sum_{i=1}^{N} l^{(i)2} n_{02}^{(i)} n_{01}^{(i)} k_{12}^{(i)}, \tag{28}$$

$$C_{13}^{\mathrm{H}} = \frac{1}{\Omega}\sum_{i=1}^{N} l^{(i)2} n_{03}^{(i)} n_{01}^{(i)} k_{13}^{(i)}, \qquad C_{14}^{\mathrm{H}} = \frac{1}{2\Omega}\sum_{i=1}^{N} l^{(i)2} n_{01}^{(i)} \left(n_{03}^{(i)} k_{12}^{(i)} + n_{02}^{(i)} k_{13}^{(i)}\right), \tag{29}$$

$$C_{15}^{\mathrm{H}} = \frac{1}{2\Omega}\sum_{i=1}^{N} l^{(i)2} n_{01}^{(i)} \left(n_{03}^{(i)} k_{11}^{(i)} + n_{01}^{(i)} k_{13}^{(i)}\right), \qquad C_{16}^{\mathrm{H}} = \frac{1}{2\Omega}\sum_{i=1}^{N} l^{(i)2} n_{01}^{(i)} \left(n_{02}^{(i)} k_{11}^{(i)} + n_{01}^{(i)} k_{12}^{(i)}\right), \tag{30}$$

$$C_{22}^{\mathrm{H}} = \frac{1}{\Omega}\sum_{i=1}^{N} l^{(i)2} n_{02}^{(i)2} k_{22}^{(i)}, \qquad C_{23}^{\mathrm{H}} = \frac{1}{\Omega}\sum_{i=1}^{N} l^{(i)2} n_{03}^{(i)} n_{02}^{(i)} k_{23}^{(i)}, \tag{31}$$

$$C_{24}^{\mathrm{H}} = \frac{1}{2\Omega}\sum_{i=1}^{N} l^{(i)2} n_{02}^{(i)} \left(n_{02}^{(i)} k_{23}^{(i)} + n_{03}^{(i)} k_{22}^{(i)}\right), \qquad C_{25}^{\mathrm{H}} = \frac{1}{2\Omega}\sum_{i=1}^{N} l^{(i)2} n_{02}^{(i)} \left(n_{03}^{(i)} k_{12}^{(i)} + n_{01}^{(i)} k_{23}^{(i)}\right),$$

$$C_{26}^{\mathrm{H}} = \frac{1}{2\Omega}\sum_{i=1}^{N} l^{(i)2} n_{02}^{(i)} \left(n_{02}^{(i)} k_{12}^{(i)} + n_{01}^{(i)} k_{22}^{(i)}\right), \qquad C_{33}^{\mathrm{H}} = \frac{1}{\Omega}\sum_{i=1}^{N} l^{(i)2} n_{03}^{(i)2} k_{33}^{(i)}, \tag{32}$$

$$C_{34}^{\mathrm{H}} = \frac{1}{2\Omega}\sum_{i=1}^{N} l^{(i)2} n_{03}^{(i)} \left(n_{03}^{(i)} k_{23}^{(i)} + n_{02}^{(i)} k_{33}^{(i)}\right), \tag{33}$$

$$C_{44}^{\mathrm{H}} = \frac{1}{4\Omega}\sum_{i=1}^{N} l^{(i)2} \left(n_{03}^{(i)2} k_{22}^{(i)} + 2 n_{02}^{(i)} n_{03}^{(i)} k_{23}^{(i)} + n_{02}^{(i)2} k_{33}^{(i)}\right), \tag{34}$$

$$C_{45}^{\mathrm{H}} = C_{54}^{\mathrm{H}} = \frac{1}{4\Omega}\sum_{i=1}^{N} l^{(i)2} \left(n_{03}^{(i)2} k_{12}^{(i)} + n_{02}^{(i)} n_{03}^{(i)} k_{13}^{(i)} + n_{03}^{(i)} n_{01}^{(i)} k_{23}^{(i)} + n_{02}^{(i)} n_{01}^{(i)} k_{33}^{(i)}\right), \tag{35}$$

$$C_{55}^{\mathrm{H}} = \frac{1}{4\Omega}\sum_{i=1}^{N} l^{(i)2} \left(n_{03}^{(i)2} k_{11}^{(i)} + 2 n_{01}^{(i)} n_{03}^{(i)} k_{13}^{(i)} + n_{01}^{(i)2} k_{33}^{(i)}\right). \tag{36}$$

The homogenized effective stiffness of a truss core material can be obtained for Timoshenko beam members by replacing the elementary stiffness matrix formulation of Euler–Bernoulli beam by Timoshenko beam formulation in Eqs. (22)–(25). For simplicity, only results for Euler–Bernoulli beams will be presented below.

3. Analysis of truss-cored sandwich panels

3.1. Theoretical development

The structural modeling of sandwich plates and shells, as reviewed by Hohe and Librescu (2004), can be divided into two categories: multilayer theories and effective single-layer models. Multilayer theories deal with the principal layers of the sandwich structures separately and impose appropriate continuity constraints at the interfaces to satisfy the necessary compatibility of the mechanical fields with respect to the adjacent layers. Effective single-layer models use one single displacement expansion through the entire thickness of the multilayer structures. Even though multilayer theories can provide more accurate predictions on the behaviors of sandwich structures, they are more difficult to be implemented for a large number of independent field variables are involved. In comparison, effective single-layer models in general involve fewer field variables but have more accuracy losses in predictions. Therefore, lots of work have been devoted to improve the accuracy based on first order shear deformable deformation theories (FOSDT) or more higher order shear deformation theories (see, e.g., Altenbach, 2000; Vinson, 2005).

Since the purpose of the present study is to explore the optimal design of truss-cored sandwich panels, it is beyond the scope of this paper to compare the predictabilities of different theories. For simplicity, an effective single-layer model (2D sandwich model) is employed (Kollar and Springer, 2003). The effectiveness of this

model is demonstrated with the numerical examples presented in Section 5, where 2D sandwich models are compared with discrete 3D (non-homogenized) sandwich models (see Fig. 1).

The following fundamental assumptions are used for the 2D sandwich model:

– The upper and lower faces have equal transverse deflections, implying zero transverse flexibility of the core;
– The distribution of longitudinal displacement across the height of the core is linear.

The behavior of a thin plate undergoing small deformations may be analyzed by the Kirchhoff hypothesis: the normals remain straight and perpendicular to the deformed reference plane. For a sandwich plate, the first assumption is reasonable. The second may no longer be valid, however, because the normals do not necessarily remain perpendicular to the reference plane. Based on these considerations, the stain-displacement relationships in the coordinates $\bar{x}$, $\bar{y}$, $\bar{z}$ (Fig. 4) may be written as

$$\varepsilon_{\bar{x}} = \frac{\partial u}{\partial \bar{x}} = \frac{\partial u^0}{\partial \bar{x}} - \bar{z}\kappa_{\bar{x}}, \tag{37}$$

$$\varepsilon_{\bar{y}} = \frac{\partial v}{\partial \bar{y}} = \frac{\partial v^0}{\partial \bar{y}} - \bar{z}\kappa_{\bar{y}}, \tag{38}$$

$$\gamma_{\bar{x}\bar{y}} = \frac{\partial u}{\partial \bar{y}} + \frac{\partial v}{\partial \bar{x}} = \frac{\partial u^0}{\partial \bar{y}} + \frac{\partial v^0}{\partial \bar{x}} + \bar{z}\kappa_{\bar{x}\bar{y}}, \tag{39}$$

$$\gamma_{\bar{x}\bar{z}} = \frac{\partial w^0}{\partial \bar{x}} - \chi_{\bar{x}\bar{z}}, \qquad \gamma_{\bar{y}\bar{z}} = \frac{\partial w^0}{\partial \bar{y}} - \chi_{\bar{y}\bar{z}}, \tag{40}$$

$$\kappa_{\bar{x}} = \frac{\partial \chi_{\bar{x}\bar{z}}}{\partial \bar{x}}, \qquad \kappa_{\bar{y}} = \frac{\partial \chi_{\bar{y}\bar{z}}}{\partial \bar{y}}, \qquad \kappa_{\bar{x}\bar{y}} = -\frac{\partial \chi_{\bar{x}\bar{z}}}{\partial \bar{y}} - \frac{\partial \chi_{\bar{y}\bar{z}}}{\partial \bar{x}}, \tag{41}$$

$$\varepsilon^0_{\bar{x}} = \frac{\partial u^0}{\partial \bar{x}}, \qquad \varepsilon^0_{\bar{y}} = \frac{\partial u^0}{\partial \bar{y}}, \qquad \gamma^0_{\bar{x}\bar{y}} = \frac{\partial u^0}{\partial \bar{y}} + \frac{\partial v^0}{\partial \bar{x}}, \tag{42}$$

where the superscript '0' denotes quantities associated with the reference plane; $\varepsilon_{\bar{x}}$, $\varepsilon_{\bar{y}}$ and $\gamma_{\bar{x}\bar{y}}$ are the membrane strains; $\gamma_{\bar{x}\bar{z}}$, $\gamma_{\bar{y}\bar{z}}$ are the transverse shear strains; $\chi_{\bar{x}\bar{z}}$, $\chi_{\bar{y}\bar{z}}$ are the rotations of the normal in the $\bar{x}$–$\bar{z}$ and $\bar{y}$–$\bar{z}$ planes;

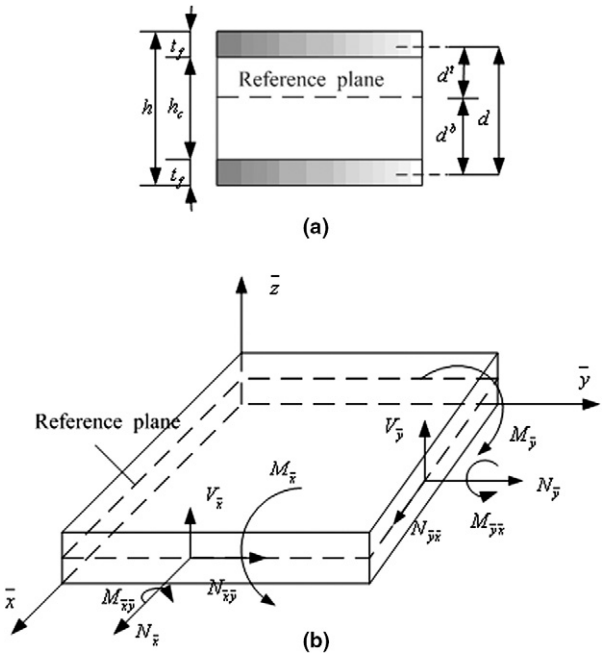

Fig. 4. Sandwich plate with identical top and bottom facesheets: (a) geometry; (b) forces and moments at reference plane.

u, v, w are the displacements in the $\bar{x}$, $\bar{y}$, $\bar{z}$ directions; and $\kappa_{\bar{x}}$, $\kappa_{\bar{y}}$, $\kappa_{\bar{x}\bar{y}}$ are the curvatures of the reference plane in the absence of shear deformation. Therefore, as shown in Fig. 4, the in-plane forces N, the moments M and the transverse shear forces V can be written as (Kollar and Springer, 2003)

$$\begin{Bmatrix} N_{\bar{x}} \\ N_{\bar{y}} \\ N_{\bar{x}\bar{y}} \end{Bmatrix} = \mathbf{A}\begin{Bmatrix} \varepsilon^0_{\bar{x}} \\ \varepsilon^0_{\bar{y}} \\ \gamma^0_{\bar{x}\bar{y}} \end{Bmatrix} + \overline{\mathbf{B}}\begin{Bmatrix} \kappa_{\bar{x}} \\ \kappa_{\bar{y}} \\ \kappa_{\bar{x}\bar{y}} \end{Bmatrix}, \tag{43}$$

$$\begin{Bmatrix} M_{\bar{x}} \\ M_{\bar{y}} \\ M_{\bar{x}\bar{y}} \end{Bmatrix} = \overline{\mathbf{B}}\begin{Bmatrix} \varepsilon^0_{\bar{x}} \\ \varepsilon^0_{\bar{y}} \\ \gamma^0_{\bar{x}\bar{y}} \end{Bmatrix} + \mathbf{D}\begin{Bmatrix} \kappa_{\bar{x}} \\ \kappa_{\bar{y}} \\ \kappa_{\bar{x}\bar{y}} \end{Bmatrix}, \tag{44}$$

$$\begin{Bmatrix} V_{\bar{x}} \\ V_{\bar{y}} \end{Bmatrix} = \widetilde{\mathbf{S}}\begin{Bmatrix} \gamma_{\bar{x}\bar{z}} \\ \gamma_{\bar{y}\bar{z}} \end{Bmatrix}, \tag{45}$$

where $\mathbf{A}$, $\overline{\mathbf{B}}$ and $\mathbf{D}$ are the in-plane stiffness matrices of the sandwich, and $\widetilde{\mathbf{S}}$ is its shear stiffness matrix.

To evaluate the above stiffness matrices, the following considerations are in general necessary: (a) The assumption of *weak* core and *strong* core sandwich structures should be justified. For the former the core is capable of carrying transverse shear loading only, whereas for the latter the core can carry both in-plane and out-of-plane forces. (b) *Thin* facesheets should be distinguished from *thick* facesheets. In the former case, the facesheets are treated as membranes (with negligible bending and transverse shear deformations), whereas those in the latter can carry both in-plane and out-of-plane forces. Detailed examination of these scenarios will be left for future studies; here, for simplicity, the same assumptions used by Wicks and Hutchinson (2001) are made, namely, the stiffness matrices are evaluated by assuming that the in-plane stiffnesses of the core and the out-of-plane stiffnesses of the facesheets are both negligible.

Under these assumptions, the $\mathbf{A}$, $\overline{\mathbf{B}}$ and $\mathbf{D}$ stiffness matrices of the sandwich plate are governed solely by the stiffnesses of the faces. Especially, when the top and bottom faces are identical and their layup is symmetrical with respect to the midplane of each face, we have:

$$\mathbf{A} = 2\mathbf{A}^*, \qquad \overline{\mathbf{B}} = \mathbf{0}, \qquad \mathbf{D} = \tfrac{1}{2}d^2\mathbf{A}^* + 2\mathbf{D}^*, \tag{46}$$

where $\mathbf{A}^*$ and $\mathbf{D}^*$ are evaluated in a coordinate system whose origin is located at the reference plane of each face, $d = h_c + t_f$ is the distance between the midplanes of faces, h_c is the thickness of sandwich core and h_f is the thickness of face (Fig. 4). Furthermore, to evaluate the shear stiffness matrix $\widetilde{\mathbf{S}}$, it is assumed that the faces are thin and hence its shear deformation is negligible. Thus, the relationship between the average shear deformation of the sandwich plate and the deformation of the core is given by

$$\gamma^c_{\bar{x}\bar{z}} = \frac{d}{h_c}\gamma_{\bar{x}\bar{z}}, \qquad \gamma^c_{\bar{y}\bar{z}} = \frac{d}{h_c}\gamma_{\bar{y}\bar{z}}, \tag{47}$$

from which the shear stiffness matrix $\widetilde{\mathbf{S}}$ can be written as

$$\widetilde{\mathbf{S}} = \frac{d^2}{h_c}\sum_{i=1}^{N}\widetilde{\mathbf{S}}^i = \frac{d^2}{h_c}\begin{bmatrix} C^H_{55} & C^H_{45} \\ C^H_{45} & C^H_{44} \end{bmatrix}, \tag{48}$$

where $C^H_{\alpha\beta}$ $(\alpha, \beta = 4, 5)$ are the homogenized moduli of the core material given in Eqs. (34)–(36), and N is the total number of truss members in the unit cell.

3.2. Finite element implementation

To check the validity of effective single-layer sandwich models with homogenized cores, finite element (FE) analysis was performed on a benchmark problem (see Section 5.1), using single-layer sandwich models based FE model (2D model) and discrete 3D sandwich models based FE model (3D model), respectively. The multi-layered 8-node isoparametric shell elements (Shell 91) in ANSYS code (ANSYS, 2003) is selected for single-layer sandwich FE models, which was developed based on the works of Ahmad et al. (1970) and Cook (1981).

Manet (1998) used three kinds of FE models in ANSYS, including Shell 91, to calculate the behavior of sandwich structures. The results showed Shell 91 had good performance in numerical simulations.

In 3D sandwich FE model, truss core sandwiches are modeled by the assembly of 4-node quadrilateral shell elements (Shell 63) for facesheets and 2-node Euler–Bernoulli beam elements (Beam44) or 2-node Timoshenko beam elements (Beam188) for rods in truss core.

4. Optimization of truss-cored sandwiches

The design optimization of a periodic truss-cored sandwich system aims to find the optimal unit cell topology with minimum system weight when subjected to loading. Three different kinds of design variables are optimized: topological, shaping and sizing variables. The topological variables determine the optimum number of truss elements in a unit cell. For the cubic unit cell configuration as shown in Fig. 5, the shaping variables are the total thickness h of the sandwich (for thin facesheets, $h \approx h_c$), the width D of the unit cell (identical width in the two transverse directions assumed in this paper), and the coordinates $(\bar{\mathbf{x}}, \bar{\mathbf{y}}, \bar{\mathbf{z}})$ of the top and bottom ends of the truss elements in the unit cell. The sizing variables are the facesheet thickness t_f (identical thickness of top and bottom facesheets assumed), the rod radius R_c for solid truss members or the outer rod radius R_c and inner radius r_c for hollow truss members. All the truss members are assumed to have the same values of the sizing variables.

Design optimizations of truss-cored sandwiches are investigated below using the sandwich model described in Sections 2 and 3. Truss-cored sandwich plates subjected to bending and transverse shear loads and subjected to in-plane compression loading are optimized separately. In addition to solid truss systems, based on the feasibility of fabricating truss systems with hollow truss members, as discussed in Wadley et al. (2003), the pyramidal truss core sandwich plates with hollow truss members (Fig. 5(b)) are optimized.

4.1. Design optimization of sandwich plates subjected to bending and transverse shear

The design optimization of a truss-cored sandwich plate under three-point loading, with force per unit length, $2P$, at the center, as shown in Fig. 6(a), was investigated by Wicks and Hutchinson (2001). Each half of the plate carries a uniform transverse shear load per length, $V = P$, and a maximum moment per length, $M = PL_1$, at the center, where L_1 is half-length of the plate, $L_1 = M/V$. The truss core had a tetrahedral unit cell with solid truss members, as shown in Fig. 6(b). The four failure modes considered were: face yielding, face buckling, core member yielding, and core member buckling. The maximum stresses in the facesheets and the maximum truss member forces were obtained analytically using the method of sections. In Section 5.2, the analytical results of Wicks and Hutchinson (2001) will be compared with those obtained using the proposed 2D sandwich model as well as the discrete 3D model.

In Wicks and Hutchinson (2001), only sizing design variables were considered. Here, based on the proposed 2D computational model, both sizing and shaping design variables are included in the design optimization. For a sandwich plate under 3-point bending (Fig. 6(a)) and the corresponding cubic unit cell with solid truss members or pyramidal unit cell with hollow truss members (Fig. 5), the dimensionless design variables are:

$$\vec{\mathbf{X}} = [X_1, X_2, X_3, X_4, \mathbf{X}_5, \mathbf{X}_6, X_7]^{\mathrm{T}} = \left[\frac{t_f}{L_1}, \frac{R_c}{L_1}, \frac{h_c}{L_1}, \frac{D}{L_1}, \frac{\bar{\mathbf{x}}}{L_1}, \frac{\bar{\mathbf{y}}}{L_1}, \frac{r_c}{L_1}\right]^{\mathrm{T}}, \tag{49}$$

$$\mathbf{X}_5/X_4 \leqslant \mathbf{1}, \qquad \mathbf{X}_6/X_4 \leqslant \mathbf{1},$$

$$\mathbf{X}_5 = \left[\left(X_{51}^{\mathrm{L}}, X_{51}^{\mathrm{u}}\right), \ldots, \left(X_{5\alpha}^{\mathrm{L}}, X_{5\alpha}^{\mathrm{u}}\right), \ldots, \left(X_{5N}^{\mathrm{L}}, X_{5N}^{\mathrm{u}}\right)\right]^{\mathrm{T}},$$

$$\mathbf{X}_6 = \left[\left(X_{61}^{\mathrm{L}}, X_{61}^{\mathrm{u}}\right), \ldots, \left(X_{6\alpha}^{\mathrm{L}}, X_{6\alpha}^{\mathrm{u}}\right), \ldots, \left(X_{6N}^{\mathrm{L}}, X_{6N}^{\mathrm{u}}\right)\right]^{\mathrm{T}}, \tag{50}$$

where L_1 is the half length of the plate, subscript α denotes the αth truss member, and superscripts ('u', 'L') denote the end point of the truss intersecting on the upper and lower facesheet, respectively. Since the unit cell shape is fixed as pyramid, $\boldsymbol{X}_5$ and $\boldsymbol{X}_6$ are not active for pyramidal unit cell with hollow truss members.

For a sandwich plate under 3-point bending (Fig. 6(a)), with $t_f/h_c \ll 1$ assumed, the maximum stress in facesheets and the maximum axial compression forces of truss members can be obtained using the 2D sandwich model, as

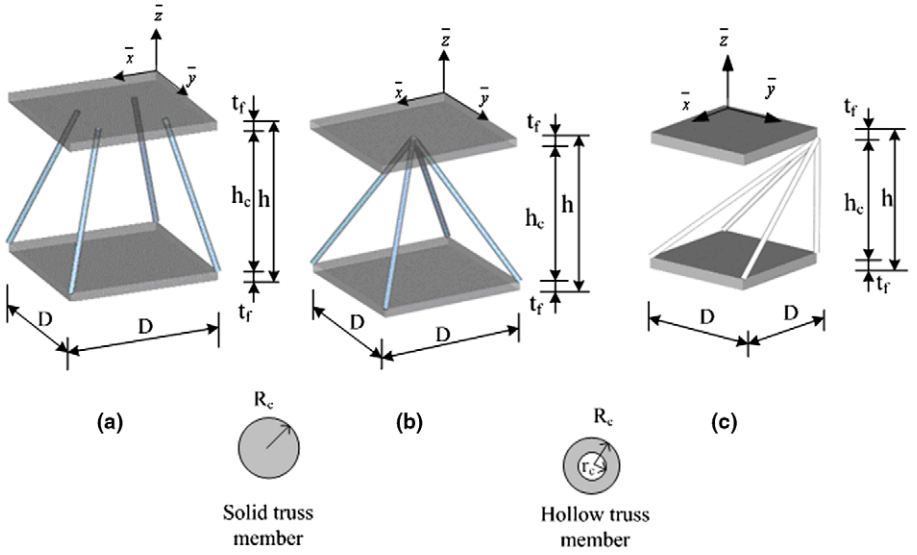

Fig. 5. Geometry of typical cubic unit cells: (a) a 4-rod unit cell, (b) a pyramidal unit cell, (c) a plagihedral pyramidal unit cell.

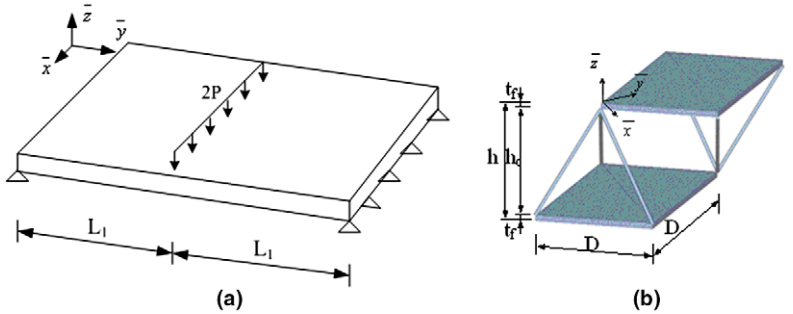

Fig. 6. Geometry of a tetrahedral truss-cored sandwich plate under three-point loading, investigated by Wicks and Hutchinson (2001) (a) a plate under three-point loading and (b) a tetrahedral unit cell with solid truss members.

$$\sigma_{\mathrm{f}} = \frac{M}{t_{\mathrm{f}} h_{\mathrm{c}}} = \left(\frac{V^2}{EM}\right)\frac{E}{X_1 X_3}, \tag{51}$$

$$F_\alpha = \frac{\pi X_2^2 L_1^2 E\left(X_{5\alpha}^{\mathrm{u}} - X_{5\alpha}^{\mathrm{L}}\right) X_3 V}{\left[\left(X_{5\alpha}^{\mathrm{u}} - X_{5\alpha}^{\mathrm{L}}\right)^2 + \left(X_{6\alpha}^{\mathrm{u}} - X_{6\alpha}^{\mathrm{L}}\right)^2 + X_3^2\right]\widetilde{S}_{11}} \quad \text{(cubic unit cell with solid truss members)}, \tag{52}$$

$$F_\alpha = \frac{\pi E V L_1^2 (X_2^2 - X_7^2) X_3 X_4}{\left[2X_3^2 + X_4^2\right]\widetilde{S}_{11}} \quad \text{(pyramidal unit cell with hollow truss members)}. \tag{53}$$

The transverse shear stiffness $\widetilde{S}_{11}$ appearing in (52) and (53) can be formulated from Eqs. (34)–(36) and (48) as

$$\widetilde{S}_{11} = E L_1 X_3^2 \sum_{\alpha=1}^{N} \frac{\pi X_2^2 \left(X_{5\alpha}^{\mathrm{u}} - X_{5\alpha}^{\mathrm{L}}\right)^2}{\left[\left(X_{5\alpha}^{\mathrm{u}} - X_{5\alpha}^{\mathrm{L}}\right)^2 + \left(X_{6\alpha}^{\mathrm{u}} - X_{6\alpha}^{\mathrm{L}}\right)^2 + X_3^2\right]^{3/2} X_4^2} \quad \text{(cubic unit cell with solid truss members)}, \tag{54}$$

$$\widetilde{S}_{11} = \frac{8.88 E L_1 X_3^2 \left(X_2^2 - X_7^2\right)}{\left(X_4^2 + 2X_3^2\right)^{3/2}} \quad \text{(pyramidal unit cell with hollow truss members)}. \tag{55}$$

Since the nodal shear forces and moments of truss members can be ignored (see Examples 2 and 3 of Section 5), only axial forces need to be considered in the design. The optimization problem for minimum weight design of the sandwich plate can be formulated as

$$\min W/\rho L_1 \tag{56}$$

subjected to the constraints:

$$\left(\frac{V^2}{EM}\right)\frac{1}{X_1X_3} \leqslant \frac{\sigma_Y}{E}, \quad \text{(facesheet yielding)}, \tag{57}$$

$$\left(\frac{V^2}{EM}\right)\frac{1}{X_1X_3} \leqslant \frac{\pi^2}{12(1-v^2)}\left(\frac{X_1}{X_4}\right)^2 \quad \text{(facesheet buckling)} \tag{58}$$

for cubic unit cell with solid truss members; and

$$\frac{E\left(X_{5\alpha}^{u}-X_{5\alpha}^{L}\right)X_3V}{\left[\left(X_{5\alpha}^{u}-X_{5\alpha}^{L}\right)^2+\left(X_{6\alpha}^{u}-X_{6\alpha}^{L}\right)^2+X_3^2\right]\widetilde{S}_{11}} \leqslant \sigma_Y \quad \text{(solid truss member yielding)}, \tag{59}$$

$$\frac{E\left(X_{5\alpha}^{u}-X_{5\alpha}^{L}\right)X_3V}{\left[\left(X_{5\alpha}^{u}-X_{5\alpha}^{L}\right)^2+\left(X_{6\alpha}^{u}-X_{6\alpha}^{L}\right)^2+X_3^2\right]\widetilde{S}_{11}} \leqslant \frac{k\pi^2EX_2^2L_1^2}{4l_a^2} \quad \text{(solid truss member buckling)} \tag{60}$$

for pyramidal unit cell with hollow truss members:

$$\left(\frac{V^2}{EM}\right)\frac{X_3X_4\left(X_4^2+2X_3^2\right)^{1/2}}{8.88X_3^2\left(X_2^2-X_7^2\right)} \leqslant \frac{\sigma_Y}{E} \quad \text{(hollow truss member yielding)}, \tag{61}$$

$$\left(\frac{V^2}{EM}\right)\frac{X_3X_4\left(X_4^2+2X_3^2\right)^{1/2}}{8.88X_3^2\left(X_2^2-X_7^2\right)} \leqslant \frac{k\pi^2X_2^2}{4\left(X_4^2/2+X_3^2\right)} \quad \text{(hollow truss member global buckling)}, \tag{62}$$

$$\begin{aligned}
&\frac{l_a^2\sqrt{1-v^2}}{R_c(R_c-r_c)} \geqslant 2.85: \quad \left(\frac{V^2}{EM}\right)\frac{X_3X_4\left(X_4^2+2X_3^2\right)^{1/2}}{8.88X_3^2\left(X_2^2-X_7^2\right)} \leqslant \frac{1}{\sqrt{3(1-v^2)}}\frac{(X_2-X_7)}{X_2},\\
&\frac{l_a^2\sqrt{1-v^2}}{R_c(R_c-r_c)} < 2.85: \quad \left(\frac{V^2}{EM}\right)\frac{X_3X_4\left(X_4^2+2X_3^2\right)^{1/2}}{8.88X_3^2\left(X_2^2-X_7^2\right)} \leqslant \left(1+\frac{12\left(X_4^2/2+X_3^2\right)^2(1-v^2)}{\pi^2X_2^2(X_2-X_7)^2}\right)\frac{\pi^2(X_2-X_7)^2}{12(1-v^2)\left(X_4^2/2+X_3^2\right)}\\
&\quad \text{(hollow truss member local buckling)}.
\end{aligned} \tag{63}$$

Here, W is the weight per unit area of the panel, $\alpha = (1, \ldots, N)$, l_α is the length of the αth truss member, and (E, v, σ_Y, ρ) are the Young's modulus, Poisson's ratio, yielding strength and mass density of the base material. If the facesheets and truss members are made of the same material, the dimensionless panel weight becomes:

$$\frac{W}{\rho L_1} = (cX_3 + 2X_1), \tag{64}$$

where c is the total volume fraction ratio of the truss members, given by

$$c = \sum_{a=1}^{N}\frac{\pi X_2^2\left[\left(X_{5\alpha}^{u}-X_{5\alpha}^{L}\right)^2+\left(X_{6\alpha}^{u}-X_{6\alpha}^{L}\right)^2+X_3^2\right]^{\frac{1}{2}}}{X_3X_4^2} \tag{65}$$

for cubic unit cell with solid truss members, and

$$c = \frac{2\pi\left(2X_4^2+4X_3^2\right)^{1/2}\left(X_2^2-X_7^2\right)}{X_4^2X_3} \tag{66}$$

for pyramidal unit cell with hollow truss members.

For facesheet buckling as represented by (58), the assumption of Wicks and Hutchinson (2001) is adopted: facesheet buckles between two neighboring truss member intersections if all truss members in a unit cell meet at the same node on the facesheet. If all truss members in a unit cell do not meet at the same node on a facesheet, Eq. (58) is expected to underestimate the maximum moment at buckling. Furthermore, the rotation restraining effect of truss core on the facesheets at the points of attachment is neglected, which also leads to the underestimation of the maximum moment.

For core member buckling, the factor k in (60) and (62) is adjusted to model different end conditions. The choice $k = 1$ and $k = 4$ corresponds to simply-supported and fully clamed conditions respectively, which may underestimate ($k = 1$) or overestimate ($k = 4$) the maximum allowable shear force associated with the buckling of a truss element. Following Wicks and Hutchinson (2001), $k = 1$ is selected for the present investigation.

4.1.1. Optimization results

The optimization problem is solved using a sequential linear programming algorithm embedded in a commercially available optimization solution engine iSIGHT (iSIGHT™), with the main programs coded in Matlab (Matlab™). The material parameters are fixed at $\sigma_Y/E = 0.007$ and $v = 1/3$, same as Budiansky (1999) and Wicks and Hutchinson (2001).

For solid truss systems, six different unit cell (RVE) topologies are investigated: plagihedral pyramidal unit cell, 4-rod unit cell, 5-rod unit cell, 6-rod unit cell, 7-rod unit cell, and 8-rod unit cell. Whilst the four rods in the plagihedral pyramidal unit cell meet at one common node on the top facesheet, as shown in Fig. 5(c), the rods in the other topologies do not necessarily meet at one common node. The metallic truss core sandwiches having these unit cell topologies are generally manufacturable. For the same sandwich geometry analyzed here, Wicks and Hutchinson (2001) gave minimum weight designs for the case of tetrahedral (3-rod) unit cell with solid truss members.

Fig. 7 plots the minimum sandwich weight $W/\rho L_1$ as a function of the normalized loading factor $V/(EM)^{1/2}$ over the range that the sandwich can be considered as *thin* plate. Of all the topologies considered for solid truss systems, the optimal topology is the 4-rod unit that has the least number of rods. However, the results of Fig. 7 reveal that the optimal design is not very sensitive to the topological design variables, as the sandwiches constructed using different cell topologies have similar weights. The corresponding values of the sizing and shaping design variables for the 4-rod unit cell, which is the optimal topology, are plotted in Figs. 8 and 9 as functions of $V/(EM)^{1/2}$. The active constraints over the entire range plotted are face yielding, face buckling and core buckling. As shown in Fig. 8, with the bottom ends of the rods fixed at the four bottom corners of the unit cell, the shaping design variables (i.e., coordinates of the top ends) do not vary significantly over

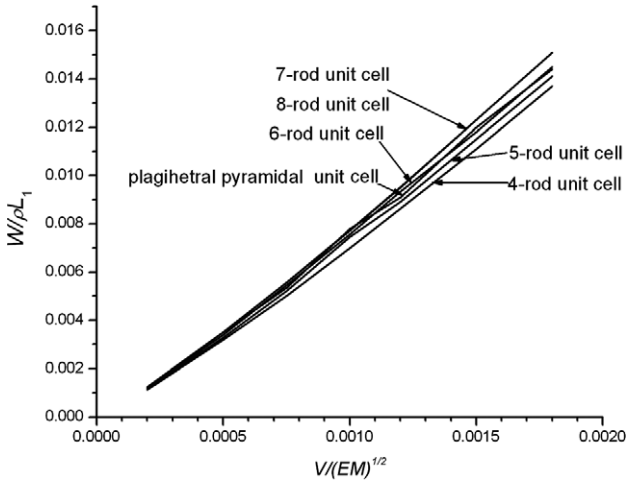

Fig. 7. Normalized weight of optimally designed truss-cored sandwich with solid truss members under 3-point bending plotted as a function of dimensionless load parameter. Two-dimensional homogenized sandwich model is used, with material properties fixed at $E/\sigma_Y = 0.007$, $v = 1/3$ and rod buckling parameter at $k = 1$.

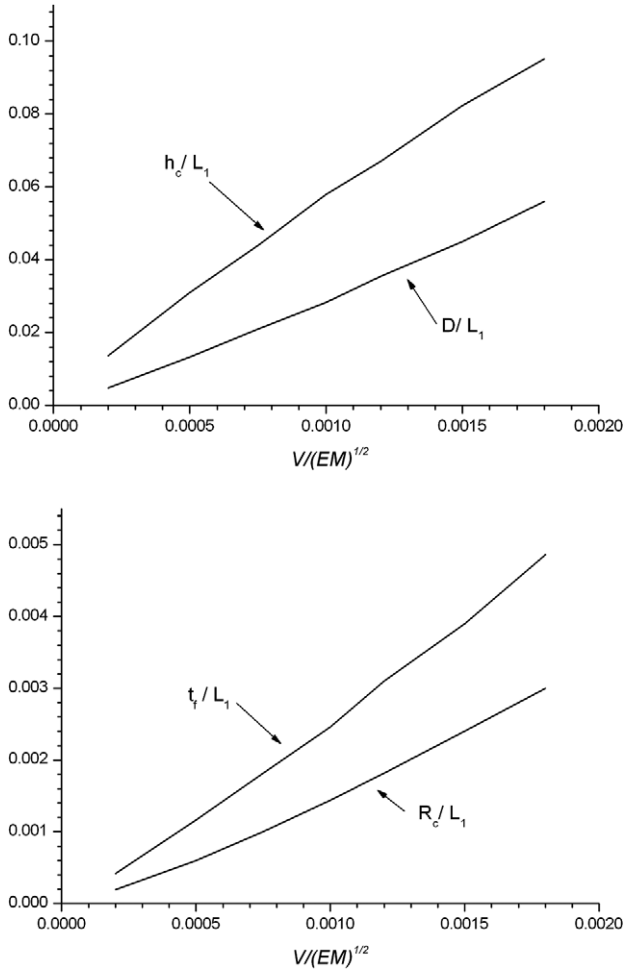

Fig. 8. Sizing design variables for optimized truss core sandwich having 4-rod unit cell and solid truss members ($E/\sigma_Y = 0.007$, $v = 1/3$, $k = 1$).

the loading range. Consequently, for obvious manufacturing reasons, these shaping design variables may be fixed at their average values.

In Fig. 10, the dimensionless weights of fully optimized truss core sandwich plates having the cubic 4-rod unit cell with solid truss members ($k = 1$) and pyramidal unit cell with hollow truss members ($k = 1$) are compared with the results given by Wicks and Hutchinson (2001) for a fully optimized truss core sandwich plate of tetrahedral unit cell and solid truss members ($k = 1$) and a fully optimized honeycomb sandwich plate. Here, all the plates are made with the same base material, with $\sigma_Y/E = 0.007$ and $v = 1/3$. Notice that truss-cored sandwiches with hollow core members outperform sandwiches made with solid truss members. For more heavily loaded plates, the pyramidal truss-cored sandwiches with hollow core members can even outperform the honeycomb-cored sandwiches, the latter generally regarded as the most structurally efficient designs under bending and/or shear loadings. The corresponding values of the sizing design variables for the pyramidal unit cell with hollow core members are plotted in Fig. 11 as functions of $V/(EM)^{1/2}$. The local buckling for hollow truss members is never active over the entire range of load parameter considered; the active constraints are face yielding, face buckling and core buckling.

As also shown in Fig. 10, although slightly heavier, sandwiches made with the 4-rod unit cell with solid truss members have similar weight advantages as the tetrahedral truss-cored sandwiches with solid truss members and the honeycomb-cored sandwiches. In the next section, it will be demonstrated that, under in-plane

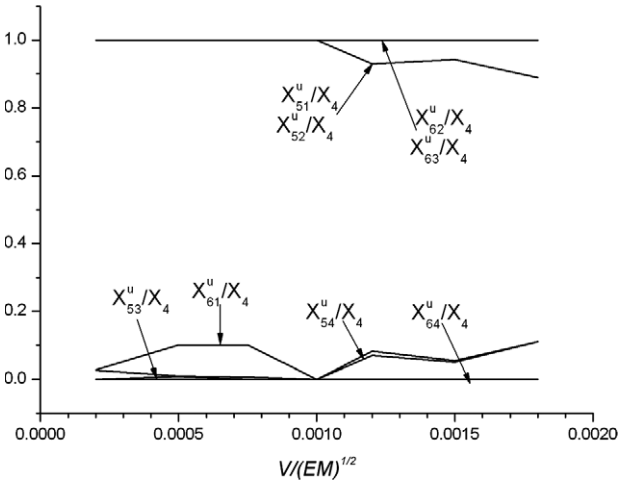

Fig. 9. Normalized shaping design variables for optimized truss core sandwich having 4-rod unit cell and solid truss members ($E/\sigma_Y = 0.007$, $v = 1/3$, $k = 1$), where $X_4 = D/L_1$, $X^u_{5\alpha} = \bar{x}^u_\alpha/L_1$, $X^u_{6\alpha} = \bar{y}^u_\alpha/L_1$, $X^L_{5\alpha} = \bar{x}^L_\alpha/L_1$, $X^L_{6\alpha} = \bar{y}^L_\alpha/L_1$, subscript α denotes the αth truss member, superscript u denotes the end of rod intersected on the top facesheet, superscript L denotes the end intersected on the bottom facesheet. The bottom ends of the four rods are fixed at four corners of the unit cell, namely, $X^L_{51} = 0$, $X^L_{61} = 0$, $X^L_{52} = 0$, $X^L_{62} = X_4$, $X^L_{53} = X_4$, $X^L_{63} = X_4$, $X^L_{54} = X_4$, $X^L_{64} = 0$.

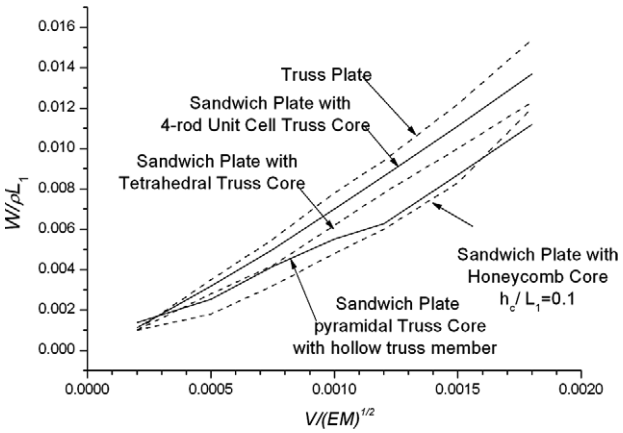

Fig. 10. Comparison of minimum weights of optimally designed sandwich plates having 4-rod unit cells with solid truss members ($k = 1$), pyramidal cored sandwich plates with hollow truss members ($k = 1$), tetrahedral cored sandwich plates with solid truss members ($k = 1$), and sandwich plates with honeycomb cores ($h_c/L_1 = 0.1$), with material properties fixed at $E/\sigma_Y = 0.007$ and $v = 1/3$. The data partly come from Wicks and Hutchinson (2001).

compression loadings, the proposed new sandwich plates with 4-rod unit cell and solid truss members have weight advantages over tetrahedral truss-cored sandwiches and hat-stiffened panels, the latter regarded as one of the most efficient structures for this application (Budiansky, 1999; Tian and Lu, 2005).

4.2. Design optimization for compression panels

Wicks and Hutchinson (2001) optimized tetrahedral truss-cored sandwich plates as compression panels. A simply supported wide plate under elastic buckling load was investigated, with four types of failure mode considered: overall buckling, facesheet yielding, facesheet bucking and localized kinking. It was found that the most frequently occurring failure modes for both heavily loaded panels and lightly loaded panels were overall buckling and local buckling.

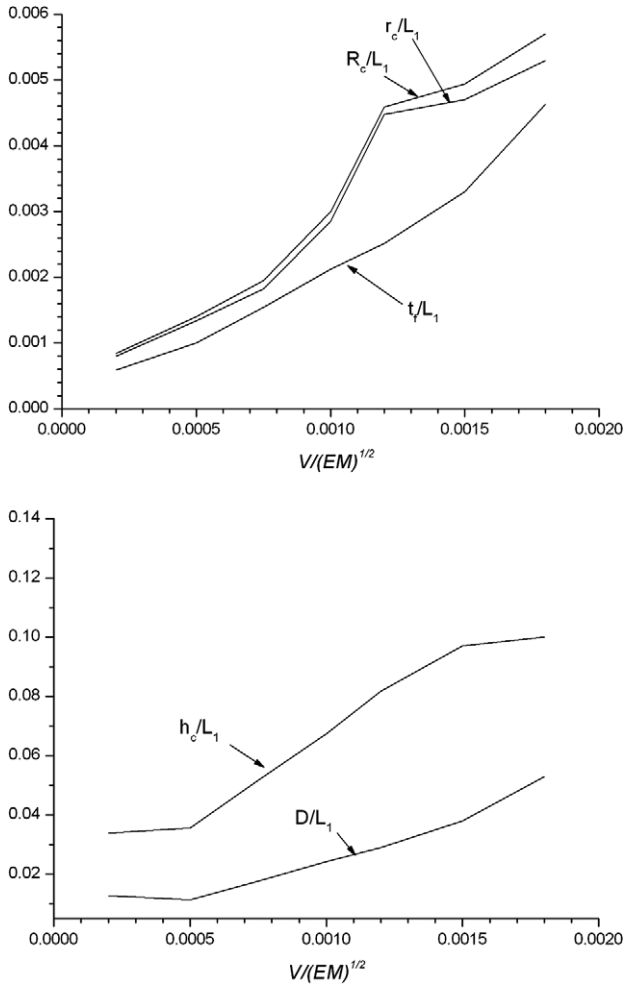

Fig. 11. Sizing design variables for the optimized pyramidal truss core sandwich with hollow truss members ($E/\sigma_Y = 0.007$, $v = 1/3$, $k = 1$).

The optimization problem for a tetrahedral truss-cored sandwich compression panel can be formulated as (Wicks and Hutchinson, 2001)

$$\min W \tag{67}$$

subjected to the constraints

$$P \leqslant P_{cr} \quad \text{(overall buckling)}, \tag{68}$$
$$P \leqslant 2\sigma_Y t_f \quad \text{(facesheet yielding)}, \tag{69}$$
$$P \leqslant P_{fcr} \quad \text{(facesheet buckling)}, \tag{70}$$
$$P \leqslant \widetilde{S}_{11} \quad \text{(localized kinking)}, \tag{71}$$

where P_{cr} is the critical buckling load of the sandwich plate, given by (Kollar and Springer, 2003)

$$P_{cr} = \left(\frac{\pi^2 D_{11}}{L^2}\right)\left(1 + \frac{\pi^2 D_{11}}{L^2 \widetilde{S}_{11}}\right)^{-1}, \tag{72}$$

P_{fcr} is the critical load for facesheet buckling:

$$P_{\mathrm{fcr}} = \frac{49}{216}\frac{\pi^2}{(1-v^2)}\frac{Et_{\mathrm{f}}^3}{\left(l_{\mathrm{a}}^2 - h_{\mathrm{c}}^2\right)}, \tag{73}$$

and

$$\widetilde{S}_{11} = \frac{62800R_{\mathrm{c}}^2 Eh_{\mathrm{c}}^2\left(374989l_{\mathrm{a}}^2 + 11h_{\mathrm{c}}^2\right)}{51963l_{\mathrm{a}}^3\left(249989l_{\mathrm{a}}^2 + 11h_{\mathrm{c}}^2\right)} \approx 1.8129\frac{R_{\mathrm{c}}^2 Eh_{\mathrm{c}}^2}{l_{\mathrm{a}}^3} \tag{74}$$

In (72), L is the length of the compression panel, and D_{11} is the component of $\mathbf{D}$ in Eq. (46):

$$D_{11} = \tfrac{1}{2}Et_{\mathrm{f}}(h_{\mathrm{c}} + t_{\mathrm{f}})^2 \cong \tfrac{1}{2}Et_{\mathrm{f}}h_{\mathrm{c}}^2. \tag{75}$$

Design optimizations for truss-core compression panels with cell topologies other than tetrahedral can be carried out using the same procedures as outlined above. In Wicks and Hutchinson (2001), only sizing design variables were analyzed. Based on the present 2D sandwich models, both sizing and shaping design variables can be considered simultaneously. In terms of dimensionless design variables and with L_1 replaced with L in Eq. (49), Eqs. (68)–(71) can be rewritten as

$$\frac{1}{2}\left(\frac{P}{EL}\right)\left(\frac{E}{\sigma_{\mathrm{Y}}}\right)X_1^{-1} \leqslant 1 \quad \text{(facesheet yielding)}, \tag{76}$$

$$\left(\frac{P}{EL}\right)\frac{6(1-v^2)}{\pi^2}X_1^{-3}X_4^2 \leqslant 1 \quad \text{(facesheet buckling)}. \tag{77}$$

For cubic unit cell with solid truss members:

$$\left(\frac{P}{EL}\right)X_1^{-1}X_3^{-2}\left(\frac{2}{\pi^2} + \frac{X_1}{\sum_{\alpha=1}^{N}\frac{\pi X_2^2\left(X_{5\alpha}^{\mathrm{u}} - X_{5\alpha}^{\mathrm{L}}\right)^2}{\left[\left(X_{5\alpha}^{\mathrm{u}} - X_{5\alpha}^{\mathrm{L}}\right)^2 + \left(X_{6\alpha}^{\mathrm{u}} - X_{6\alpha}^{\mathrm{L}}\right)^2 + X_3^2\right]^{3/2}X_4^2}}\right) \leqslant 1 \quad \text{(overall buckling)}, \tag{78}$$

$$\left(\frac{P}{EL}\right)\left(\sum_{\alpha=1}^{N}\frac{\pi X_2^2X_3^2\left(X_{5\alpha}^{\mathrm{u}} - X_{5\alpha}^{\mathrm{L}}\right)^2}{\left[\left(X_{5\alpha}^{\mathrm{u}} - X_{5\alpha}^{\mathrm{L}}\right)^2 + \left(X_{6\alpha}^{\mathrm{u}} - X_{6\alpha}^{\mathrm{L}}\right)^2 + X_3^2\right]^{3/2}X_4^2}\right)^{-1} \leqslant 1 \quad \text{(localized kinking)}. \tag{79}$$

For pyramidal unit cell with hollow truss members:

$$\left(\frac{P}{EL}\right)X_1^{-1}X_3^{-2}\left(\frac{2}{\pi^2} + \frac{X_1\left(X_4^2 + 2X_3^2\right)^{3/2}}{8.88\left(X_2^2 - X_7^2\right)}\right) \leqslant 1 \quad \text{(overall buckling)}, \tag{80}$$

$$\left(\frac{P}{EL}\right)\left(\frac{8.88X_3^2\left(X_2^2 - X_7^2\right)}{\left(X_4^2 + 2X_3^2\right)^{3/2}}\right)^{-1} \leqslant 1 \quad \text{(localized kinking)}. \tag{81}$$

The prescribed dimensionless loading parameter is P/EL, and the material properties are fixed such that $\sigma_{\mathrm{Y}}/E = 0.007$ and $v = 1/3$.

For the same unit cell topologies with solid truss members considered in Section 4.1, the minimum weights of truss core sandwiches are presented in Fig. 12. Again, the range of load parameter has been chosen to be consistent with the conditions that the panel is relatively thin. The results of Fig. 11 show that, for the construction of sandwich compression panels, unit cells with 4–8 rods not necessarily joining at a common node are superior to the plagihedral pyramidal unit cell, and the difference between a panel made with the 4-rod cell and that with a cell containing more than 4 rods is negligibly small. Therefore, only results concerning 4-rod unit cell truss core sandwich panels will be presented hereafter.

For compression panels, hat-stiffened plates have traditionally been regarded as one of the most efficient constructions (Budiansky, 1999; Tian and Lu, 2005). Recently, however, Wicks and Hutchinson (2001) demonstrated that sandwich panels with tetrahedral core and solid truss members outperform hat-stiffened single

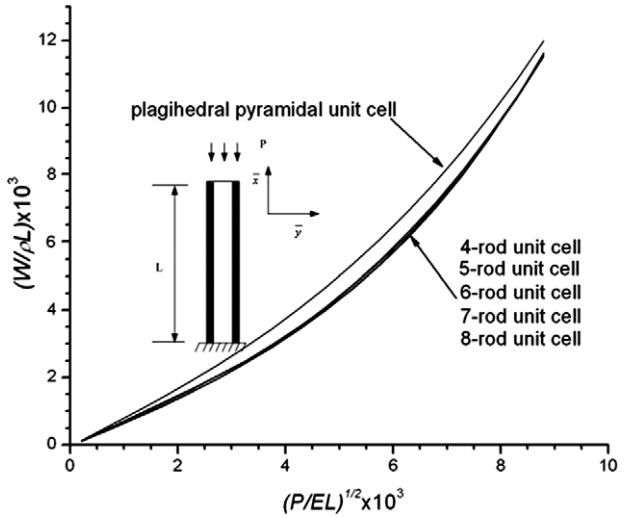

Fig. 12. Normalized weight plotted as a function of dimensionless load parameter for optimally designed truss-cored sandwich panels with solid truss members under axial compression ($E/\sigma_Y = 0.007$, $v = 1/3$). Two-dimensional homogenized sandwich model is used with the method of finite element for the prediction.

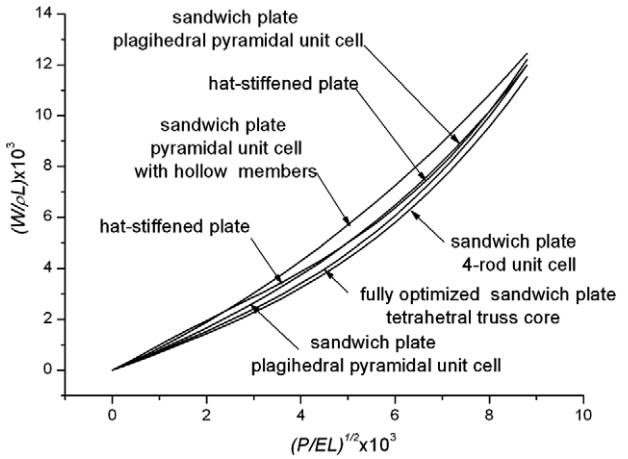

Fig. 13. Comparisons of minimum weights of various optimally designed truss core sandwich panels and hat-stiffened single layer plate under end compression ($E/\sigma_Y = 0.007$, $v = 1/3$).

layer plates. It would therefore be interesting to see how the 4-rod unit cell truss core sandwiches with solid truss members and pyramidal truss-cored sandwiches with hollow truss members compete with the above two types of benchmark compression panel. Such a comparison is presented in Fig. 13, and it is seen that although the performances of these panels are very close, the 4-rod unit cell truss core sandwiches with solid truss members indeed have weight advantages over even the tetrahedral-cored sandwiches. On the other hand, even though a pyramidal truss-cored sandwich with hollow truss members has superior performances when subjected to bending and transverse shear, as shown in Fig. 10, its performances under axial compression are not as good as other compression panels plotted in Fig. 13. Therefore, it can be deduced that pyramidal truss-cored sandwiches with either hollow or solid truss members are not the best choice for compression panels.

For the optimized 4-rod unit cell truss core sandwich with solid truss members, Fig. 14 plots the variations of its size variables with the loading parameter P/EL. It is noticed that h_c/L approaches 1/10 at the upper end

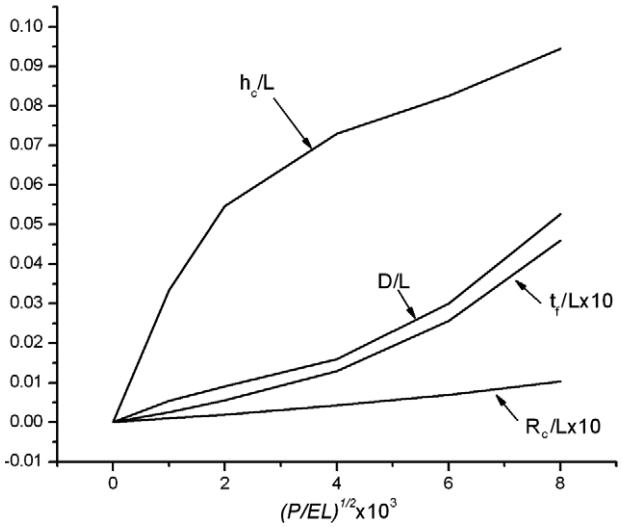

Fig. 14. Sizing design variables for the optimized 4-rod cell truss core sandwich compression panels with solid core members ($E/\sigma_Y = 0.007$, $v = 1/3$).

of the loading parameter range, i.e., when the panel is heavily loaded. The local kinking mode is never active over the entire range of load parameter considered. The more lightly loaded panels buckle at the design load simultaneously in the overall and localized modes, but are stressed below face yielding. The normalized core height h_c/L is significantly larger than the normalized unit cell width D/L for the more lightly loaded panels, which aims to resist against buckling deformation. In comparison, the more heavily loaded compression panels have three of the constraints active: overall buckling, facesheet buckling and facesheet yielding.

For the 4-rod truss core compression panels with solid truss members shown in Fig. 13, the shape design variables (namely, the coordinates of the top ends of the 4 rods in the unit cell) are plotted in Fig. 15; during the calculations, the bottom ends of the rods are fixed at the four bottom corners of the unit cell. Similar to the

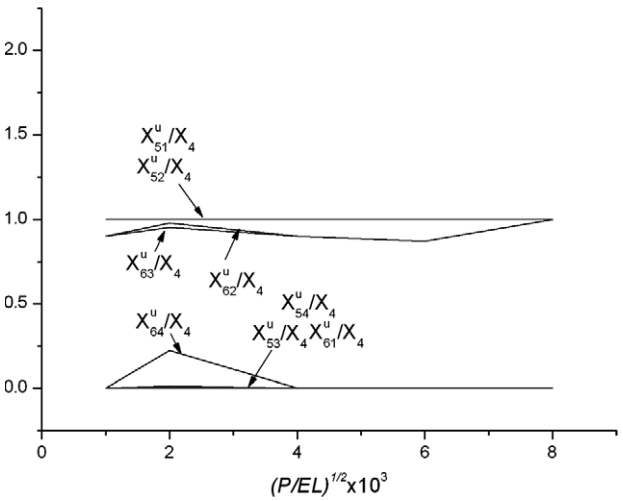

Fig. 15. Shaping design variables for the optimized 4-rod cell truss core sandwich compression panels with solid core members ($E/\sigma_Y = 0.007$, $v = 1/3$), where $X_4 = D/L_1$, $X^u_{5\alpha} = \bar{x}^u_\alpha/L_1$, $X^u_{6\alpha} = \bar{y}^u_\alpha/L_1$, $X^L_{5\alpha} = \bar{x}^L_\alpha/L_1$, $X^L_{6\alpha} = \bar{y}^L_\alpha/L_1$, subscript α denotes the αth truss member, superscript u denotes the end of rod intersected on the top facesheet, superscript L denotes the end intersected on the bottom facesheet. The bottom ends of the four rods are fixed at four corners of the unit cell, namely, $X^L_{51} = 0$, $X^L_{61} = 0$, $X^L_{52} = 0$, $X^L_{62} = X_4$, $X^L_{53} = X_4$, $X^L_{63} = X_4$, $X^L_{54} = X_4$, $X^L_{64} = 0$.

case when the sandwich is subjected to a combination of bending and transverse shear loads, these shape variables do not vary vigorously as the compression load is increased. Consequently, in the next section, a compression panel having averaged shaping variables will be chosen for one of the four numerical examples studied.

5. Comparison between predictions with 2D and 3D sandwich models

In this section, the predictions using the homogenized 2D computational models are checked against those obtained using the 3D models. Four different sandwich panels with different unit cell topologies are separately studied: (a) plagihedral pyramidal; (b) tetrahedral; (c) pyramidal; (d) 4-rod. For the pyramidal core panel, the truss members are hollow, whereas those in the rest of the panels are solid.

5.1. Plagihedral pyramidal core sandwich subjected to bending and transverse shear

Truss core sandwich panels having plagihedral pyramidal cores as shown in Fig. 5(c) are analyzed using the method of finite elements with both 2D sandwich model and 3D direct computational model. In the 3D model, the facesheets and the truss core are simulated with shell elements (Shell63, Q4, in the notation of the commercially available FE code ANSYS 7.0) and 3D beam elements (Beam44, representing the Euler–Bernoulli beam), respectively. In the homogenized sandwich model (2D model), the core is assigned with the stiffness $\mathbf{C}^{\mathrm{H}}$ given in Eqs. (28)–(36) and simulated with the element Shell91 (Q8), which has an optional switch for sandwich structures analyses.

The truss core and the solid facesheets are both made of steel, with Young's modulus $E = 206$ GPa, Poisson's ratio $v = 0.3$, yield strength $\sigma_{\mathrm{Y}} = 355$ MPa, and mass density $\rho = 7850$ kg/m^3. The following geometric variables are selected: core height $h_{\mathrm{c}} = 0.04$ m; cross-sectional area of each cylindrical rod $A = 1.25 \times 10^{-5}$ m^2; facesheet thickness $t_{\mathrm{f}} = 0.00333$ m; the width D of unit cell varies from 0.01 m to 0.0333 m; the length and width of the panel are both fixed at 0.5 m. As shown in Fig. 16, the panel is clamped at two edges and subjected to two different static loading cases: Case 1 represents an out-of-plane uniform loading of $P =$ 10,000 KN/m^2 on the upper facesheet, which aims to compare the bending and transverse shear behavior of 2D and 3D sandwich models (Fig. 16(a) and (c)); Case 2 represents an in-plane compression load of $P_1 = 800$ KN/m acting on the upper facesheet only, which aims to compare the coupled behavior of bending, transverse shear and in-plane compression for the two models (Fig. 16(b) and (d)).

Fig. 17 plots the total amount of strain energy stored in the sandwich panel as a function of unit cell width D for both loading cases; the corresponding maximum nodal displacements are presented in Fig. 18 for Case 1 (Fig. 16(a) and (c)) and in Fig. 19 for Case 2 (Fig. 16(b) and (d)). These results show that the coupled behavior of in-plane compression and out-of-plane bending predicted with the 2D homogenization model agrees well with those predicted using the direct 3D computational model, although the 2D model is a slightly stiffer than the 3D model. However, the agreement between 2D and 3D model predictions for out-of-plane behavior (loading Case 1) is not as good as that for the coupled behavior, which can be attributed to two important issues:

1. The current 2D homogenized model is based on the effective single-layer sandwich approaches, which considers the in-plane deformations of the facesheets but ignores their out-of-plane deformations.
2. To ensure the same shear resultants between facesheets and truss core, closed form solutions should be formulated (Frostig, 2003).

These issues will be addressed in a separate study (Liu et al., in preparation).

5.2. Tetrahedral core sandwich under bending and transverse shear

The design optimization of a wide tetrahedral-cored sandwich plate under three-point loading, with force per unit length, $2P$, at the center, as shown in Fig. 6(a), was investigated by Wicks and Hutchinson (2001). Each half of the plate carries a uniform transverse shear load per length, $V = P$, and a maximum moment

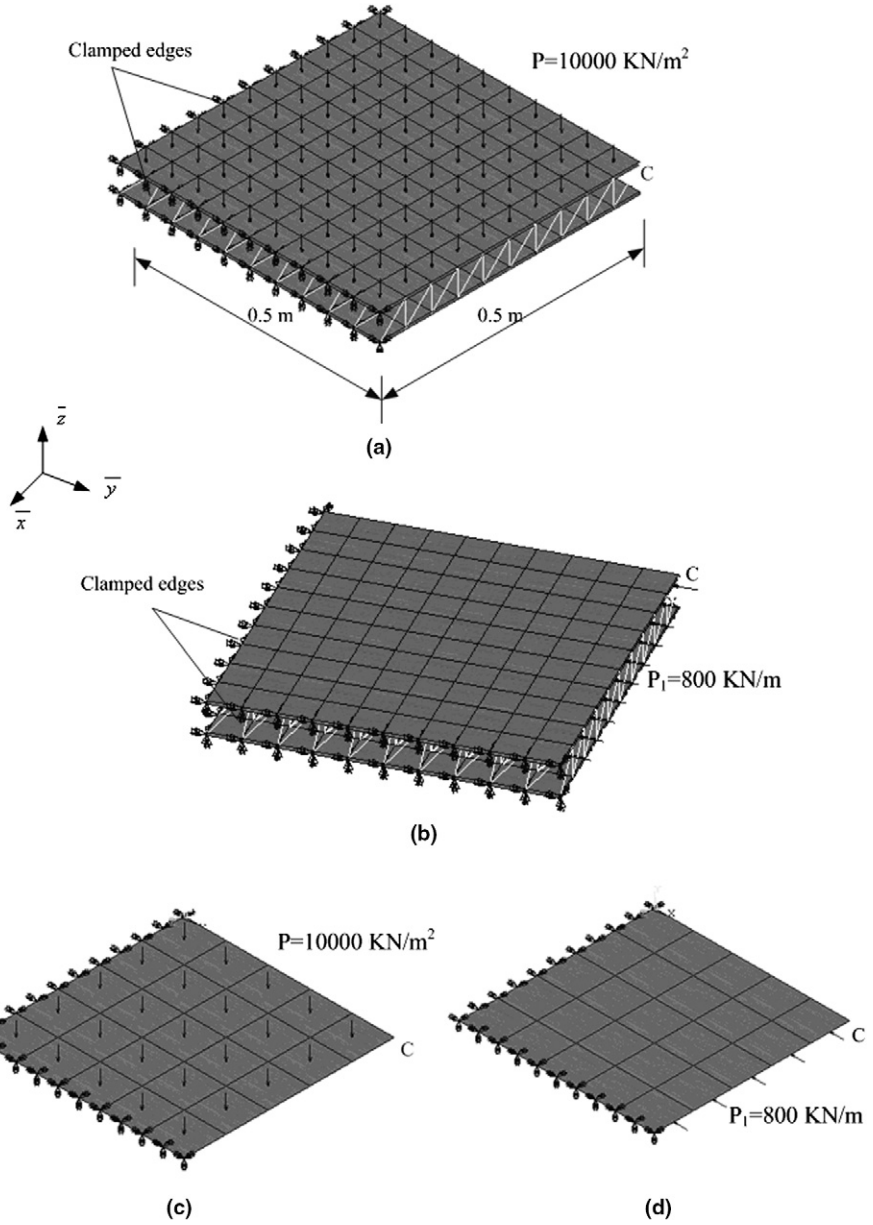

Fig. 16. Plagihedral pyramidal core sandwich: (a) 3D model for loading Case 1; (b) 3D model for loading Case 2; (c) 2D model for loading Case 1; (d) 2D model for loading Case 2. The geometry of the plagihedral pyramidal unit cell is shown as Fig. 5(c).

per length, $M = PL_1$, at the center, where L_1 is half-length of the plate, $L_1 = M/V$. The geometry of the unit cell is as shown in Fig. 6(b), which was made with solid truss members. The maximum stress σ_f in the facesheets and the maximum axial force F_c in the truss members were obtained from elementary equilibrium considerations, neglecting the small contribution from transverse shear stresses within the facesheets:

$$\sigma_f = \frac{M}{t_f h_c}, \qquad F_c = \frac{\sqrt{3}V\sqrt{l_\alpha^2 - h_c^2}\, l_\alpha}{h_c}, \tag{82}$$

where M and V denote the maximum moment and shear force per unit length, and l_α is the length of truss members. Obviously, the optimization models and optimized results are governed by Eq. (82). In this section,

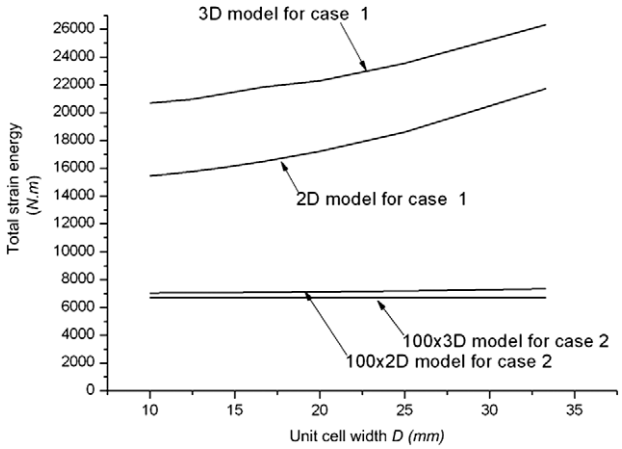

Fig. 17. Total strain energy in plagihedral pyramidal core sandwich panel plotted as a function of unit cell width D.

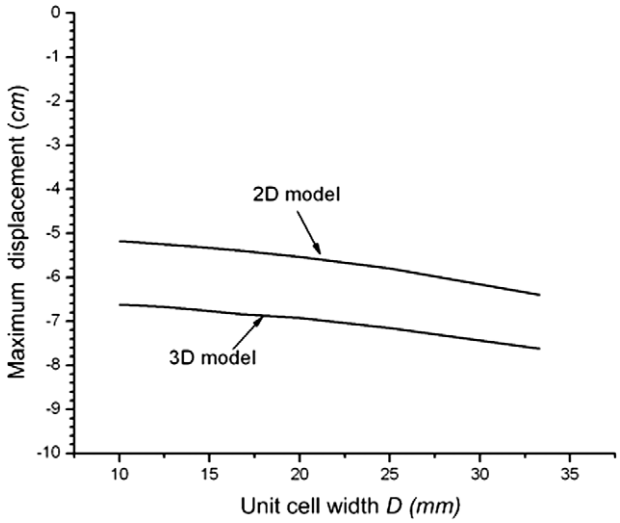

Fig. 18. Maximum node deflection of plagihedral pyramidal core sandwich panel plotted as a function of unit cell width D for loading Case 1. The maximum node deflection occurs at corner C in the $\bar{z}$-direction as shown in Fig. 16.

this problem, as mentioned above, is analyzed using the method of finite elements with both 2D sandwich model and 3D direct computational model.

For a 3-rod unit cell truss core sandwich plate, using the proposed 2D sandwich model and assuming $t_f/h_c \ll 1$, the same expression for σ_f as in Eq. (82) can be obtained. The nodal displacements and rotations of truss members can be solved from Eqs. (13), (16), (19), (45) and (48). Hence, the maximum nodal forces and moments of truss members can be solved from the corresponding equilibrium equations, as [see Fig. 3 for the definition of local coordinates (x, y, z) for a truss member]:

$$F_x = 1.7320\frac{\left(l_\alpha^2 - h_c^2\right)^{1/2} V l_a}{h_c}, \qquad F_y = 2.6\frac{V R_c^2\left(2h_c^2 - l_\alpha^2\right)}{l_a h_c^2}$$
$$F_z = 0, \qquad M_x = 0, \qquad M_y = 0, \qquad M_z = 1.3\frac{V R_c^2\left(2h_c^2 - l_\alpha^2\right)}{h_c^2}. \tag{83}$$

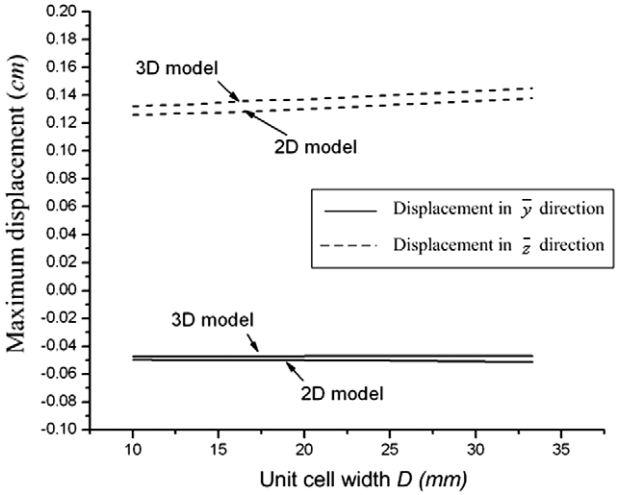

Fig. 19. Maximum node deflection of plagihedral pyramidal core sandwich panel plotted as a function of unit cell width D for loading Case 2. The maximum node displacement occurs at corner C both in the $\bar{y}$-direction and $\bar{z}$-direction as shown in Fig. 16.

Simulations with 3D finite element models are subsequently performed, with respect to three groups of loading parameters and geometry parameters, and the results are compared with those obtained from Eq. (83). The facesheets and the truss core are simulated separately with shell elements and 3D beam elements (Beam188 of ANSYS is selected, representing the Timoshenko beam, which can provide more accurate solutions for nodal forces and moments than the Euler–Bernoulli beam). The truss core and the solid facesheets are made of high strength aluminum with $E = 70$ GPa, $v = 1/3$, $\sigma_Y = 490$ MPa and mass density $\rho = 2700$ kg/m^3. The three groups of loading and geometrical parameters given in Table 1 are chosen from the normalized design parameters for optimized truss plates as shown in Figs. 7 and 8 of Wicks and Hutchinson (2001), which represent the lightly loaded plate, moderately loaded plate and heavily loaded plate, respectively. In Table 2, the results obtained by Eq. (83) and the 3D sandwich model are compared.

As shown in Table 2, the overall agreement between the 2D and 3D sandwich model predictions on maximum nodal forces and moments of truss members is good. In comparison, in Eq. (82), obtained by Wicks and Hutchinson (2001) using the elementary method of sections, only the maximum axial forces of truss members

Table 1
Three groups of loading and geometrical parameters for tetrahedral truss core sandwich plates with solid truss members subjected to bending and transverse shear, chosen from Figs. 7 and 8 of Wicks and Hutchinson (2001), with $E = 70$ GPa, $v = 1/3$ and $\sigma_Y = 490$ MPa

Case	$V/(EM)^{1/2}$	V (KN/m)	h_c (mm)	l_x (mm)	R_c (mm)	t_f (mm)
1	0.0005	13.1	24.38	28.12	0.75	0.75
2	0.0012	75.6	56.25	61.88	2.25	2.1
3	0.0018	170.1	82.5	90	3.75	3.15

Table 2
Maximum nodal forces and moments of truss members for tetrahedral truss core sandwich plates with solid truss members subjected to bending and transverse shear

Case	F_x (N)	F_y (N)	F_z (N)	M_x (N m)	M_y (N m)	M_z (N m)
1	366.70	0.46	0	0	0	0.0064
	354.16	0.429	0.392	0.00302	0.0004	0.0042
2	3714.8	42.7	0	0	0	0.04
	3686.6	41.17	1.98	0.00916	0.0286	0.00413
3	11560	56	0	0	0	0.3
	10336	57.23	1.489	0.144	0.02	0.137

The numerators and denominators refer to the results obtained with 2D and 3D models, respectively.

are available. Therefore, the 2D sandwich model appears to have the advantages in cases where the nodal shear forces and moments of truss members are not negligible. However, for all three cases considered in Tables 1 and 2, the axial force F_x dominates over other nodal forces and moments. Therefore, for *thin plates*, it is justifiable to assume that all truss members only carry axial forces, as assumed in the design optimization studies of Section 4, and in Wicks and Hutchinson (2001), Mohr (2005) and many others.

5.3. Pyramidal core sandwich with hollow truss members under bending and transverse shear

The third example is for a pyramidal core sandwich plate with hollow truss members under three-point loading, with force per unit length, $2P$, at the center, as shown in Fig. 6(a). The unit cell configuration is as shown in Fig. 5(b), with $\sigma_Y/E = 0.007$, $v = 1/3$. Using the proposed 2D sandwich model and assuming $t_f/h_c \ll 1$, the maximum stress σ_f in the facesheets and the maximum axial forces of truss members can be solved as [see Fig. 3 for the definition of local coordinates (x, y, z) for a truss member]:

$$\sigma_f = \frac{M}{t_f h_c}, \qquad F_x = \frac{0.3536 d \left(d^2 + 2h_c^2\right)^{1/2} V}{h_c}. \tag{84}$$

Simulations with 3D finite element models are subsequently performed, using three groups of loading parameters and geometry parameters (Table 3). These parameters are chosen from the normalized design parameters for optimized truss plates as shown in Fig. 11 which represent the lightly loaded plate, moderately loaded plate and heavily loaded plate, respectively. Table 4 presents the results obtained by 2D and 3D sandwich models for the same FE constructions and base material properties mentioned in Section 5.2. The overall agreement between the 2D and 3D sandwich model predictions on maximum nodal forces and moments of truss members is good.

As shown in Table 4, for all the three cases considered, the axial force F_x dominates over other nodal forces and moments. Therefore, for *thin plates* with *hollow* truss members, it is reasonable to assume that all truss members only carry axial forces, as assumed in the design optimization studies of Section 4.

5.4. Truss core sandwich with 4-rod unit cell as compression panel

The fourth example is a 4-rod unit cell sandwich plate subjected to in-plane compression. The unit cell configuration is firstly optimized using the same method as described in Section 4, with $\sigma_Y/E = 0.007$, $v = 1/3$, and

Table 3
Three groups of loading and geometrical parameters for pyramidal truss core sandwich plates with hollow truss members subjected to bending and transverse shear, chosen from Fig. 11, with $E = 70$ GPa, $v = 1/3$ and $\sigma_Y = 490$ MPa

Case	$V/(EM)^{1/2}$	V (KN/m)	h_c (mm)	D (mm)	R_c (mm)	t_f (mm)	r_c (mm)
1	0.0005	13.1	53.4	17	2.1	1.5	2.01
2	0.0012	75.6	61.35	21.75	3.44	1.9	3.36
3	0.0018	170.1	75	39.75	4.28	3.47	3.98

Table 4
Maximum nodal forces and moments of truss members for pyramidal truss core sandwich plates with hollow truss members subjected to bending and transverse shear

Case	F_x (N)	F_y (N)	F_z (N)	M_x (N m)	M_y (N m)	M_z (N m)
1	114.15	2.02	2.18	0	0.0119	0.00111
	94.16	0.239	5.14	0.0039	0.00031	0.00142
2	847.71	27.5	30.24	0	0.956	0.87
	731.24	1.4	24	0.00416	0.46	0.19
3	3610.87	66	82.2	0	3.3	2.65
	3489.78	37.28	64.89	1.18	0.028	0.637

The numerators and denominators refer to the results obtained with 2D and 3D models, respectively.

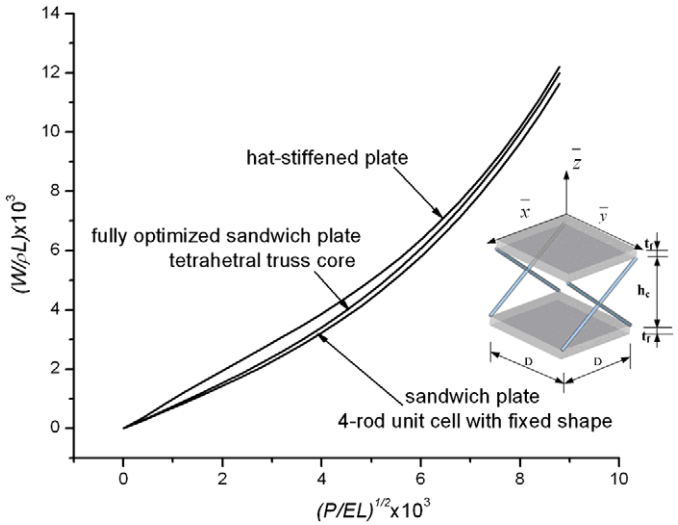

Fig. 20. Minimum weights of optimally designed compression panels: 4-rod cell truss core sandwich, tetrahedral core sandwich (Wicks and Hutchinson, 2001), and hat-stiffened single layer plate, all with ($E/\sigma_Y = 0.007$, $v = 1/3$).

Table 5
Maximum allowable compression load and corresponding failure modes for 4-rod truss core sandwich panels

Case	P/EL_1	P (KN/m)	h_c (mm)	D (mm)	R_c (mm)	t_f (mm)	P_{FEM} (KN/m)	Failure mode
1	1.6×10^{-5}	1120	72.5	16	0.4	1.3	986	Facesheet wrinkling
2	3.6×10^{-5}	2520	81	29.6	0.7	2.57	2520	Facesheet wrinkling, facesheet yielding
3	6.4×10^{-5}	4480	92	53	1.1	4.6	4480	Facesheet yielding

The loading and geometrical parameters are chosen from Fig. 14, with $E = 70$ GPa, $v = 1/3$ and $\sigma_Y = 490$ MPa and $L = 1$ m.

shape design variables fixed at the average values of Fig. 15. The morphology of the optimized unit cell is shown as the insert in Fig. 20, where the minimum weights of the 4-rod unit cell plates are compared with those of hat-stiffened plates and tetrahedral core sandwiches. The sizing design variables for the minimum weight design are similar to those plotted in Fig. 14.

To verify the results of Fig. 20, a 3D finite element model is analyzed to determine the failure modes and the corresponding maximum allowable compression load. Three groups of loading and geometrical parameters, corresponding to a lightly loaded panel, a moderately loaded panel and a heavily loaded panel, respectively, are selected from Fig. 14 ($L = 1$ m assumed) and are summarized in Table 5. The 3D finite element model construction and the base material properties are the same as in Section 5.2.

It is seen from Table 5 that there is close agreement between the results obtained with the 2D sandwich model and those with the 3D sandwich model, except for Case 1 where the load applied on the panel is relatively small. For more lightly loaded panels, the failure mode is face wrinkling, whereas for more heavily loaded panels, the failure mode is face yielding. For moderately loaded panels, both face wrinkling and face yielding are active. Since face wrinkling is sensitive to how and where the compression loads and constraints are imposed in the 3D finite element model, the maximum allowable compression load for a lightly loaded panel obtained by the 3D model (P_{FEM} in Table 5) is less than that predicted by the 2D model; see Case 1 in Table 5.

6. Concluding remarks

The minimum weight design of sandwich plates comprised of truss cores faced with solid sheets of the same material has been investigated for various prescribed combinations of bending, shear and compression.

A homogenization approach is adopted, with the periodic 3D truss cores replaced with 2D effective solid cores. The truss members are modeled using Euler–Bernoulli beams, with clamped ends assumed. The optimization is subjected to the constraints that no failure mechanism is active, including overall buckling, facesheet buckling/wrinkling, facesheet yielding, core member yielding and buckling.

Close agreement between the predictions obtained with the 2D model and those from 3D direct finite element simulations is observed, suggesting that the computationally advantageous 2D sandwich model is suitable for practical designs. It is found that the proposed simple 4-rod unit cell with solid truss members and pyramidal unit cell with hollow truss members compete well with the best cell topologies: honeycombs, tetrahedral cell and hat-stiffeners. Furthermore, it is found that, if the sandwiches can be considered as thin plates (and they usually do), the deformation of the truss members are dominated by axial forces and hence can be faithfully modeled with one-dimensional bars having pin-jointed ends.

Acknowledgements

The authors wish to thank the National Basic Research Program of China through Grant No. 2006CB601202, the National Natural Science Foundation of China through Grant Nos. 10572111 and 10572119, the National 111 Project of China (Grant No. B06024), the Program for New Century Excellent Talents in University (NCET-04-0958), the Open Foundation of State Key Laboratory of Structural Analysis of Industrial Equipment, and the Doctorate Foundation of Northwestern Polytechnical University for financial supports of this work.

References

Ahmad, S., Irons, B.M., Zienkiewicz, O.C., 1970. Analysis of thick and thin shell structures by curved finite elements. Int. J. Numer. Meth. Eng. 2, 419–451.

Allen, H.G., 1969. Analysis and Design of Structural Sandwich Panels. Pergamon, Oxford.

Altenbach, H., 2000. An alternative determination of transverse shear stiffnesses for sandwich and laminated plates. Int. J. Solids Struct. 37, 3503–3520.

ANSYS, Inc., 2003. ANSYS User's Manual.

Budiansky, B., 1999. On the minimum weights of compression panels. Int. J. Solids Struct. 36, 3677–3708.

Cook, R.D., 1981. Concepts and Applications of Finite Element Analysis, second ed. John Wiley and Sons, New York.

Deshpande, V.S., Fleck, N.A., 2001. Collapse of truss-core sandwich beams in 3-point bending. Int. J. Solids Strut. 38, 6275–6305.

Deshpande, V.S., Fleck, N.A., Ashby, M.F., 2001. Effective properties of octet-truss lattice material. J. Mech. Phys. Solids 49, 1747–1796.

Evan, A.G., Hutchinson, J.W., Fleck, N.A., Ashby, M.F., Wadley, H.N.G., 2001. The topological design of multifunctional cellular metals. Prog. Mater. Sci. 46, 309–327.

Frostig, Y., 2003. Classical and high-order computational models in the analysis of modern sandwich panels. Composites Part B 34, 83–100.

Gustafsson, R.N.G., 2000. Ultralight stainless steel sandwich materials – HSSA. In: Meyer-Piening, H.R., Zenkert, D. (Eds.), Sandwich Construction, vol. 5. EMAS, pp. 169–176.

Hill, R., 1963. Elastic properties of reinforced solids: some theoretical principles. J. Mech. Phys. Solids 11, 357–372.

Hohe, J., Becker, W., 2002. Effective stress–strain relations for two-dimensional cellular sandwich cores: Homogenization, material models, and properties. Appl. Mech. Rev. 55, 61–87.

Hohe, J., Librescu, L., 2004. Advances in the structural modeling of elastic sandwich panels. Mech. Adv. Mat. Struct. 11, 395–424.

Hutchinson, J.W., Xue, Z., 2005. Metal sandwich plates optimized for pressure impulses. Int. J. Mech. Sci. 47, 545–569.

Hyun, S., Karlson, A.M., Torquato, S., Evans, A.G., 2003. Simulated properties of Kagomé truss core panels. Int. J. Solids Strut. 40, 6989–6998.

Kim, T., Zhao, C.Y., Lu, T.J., Hudson, H.P., 2004. Convective heat dissipation with lattice-frame materials. Mech. Mater. 36, 1011–1020.

Kollar, L.P., Springer, G.S., 2003. Mechanics of Composite Structures. Cambridge University Press, Cambridge, UK.

Kooistra, G.W., Deshpande, V.S., Wadley, H.N.G., 2004. Compressive behavior of age hardenable tetrahedral lattice truss structures made from aluminum. Acta Mater. 52, 4229–4237.

Lai, W.M., Rubin, D., Krempl, E., 1993. Introduction to Continuum Mechanics, third ed. Pergamon/Elsevier Science Publisher.

Liu, J.S., Lu, T.J., 2004. Multi-objective and multi-loading optimization of ultralightweight truss materials. Int. J. Solids Strut. 41, 618–635.

Liu, T., Deng, Z.C., Lu, T.J., in preparation. On optimally designed sandwich-walled cylinders with ultralight cellular materials.

Manet, V., 1998. The use of ANSYS to calculate the behavior of sandwich structures. Compos. Sci. Technol. 58, 1899–1905.

Mohr, D., 2005. Mechanism-based multi-surface plasticity model for ideal truss lattice materials. Int. J. Solids Strut. 42, 3235–3260.

Noor, A.K., Burton, W.S., Bert, C.W., 1996. Computational models for sandwich panels and shells. Appl. Mech. Rev. 4 (3), 155–199.

Straalen, I.J.V., 2000. Comprerhensive overview of theories for sandwich panels. In: Workshop on Modeling of Sandwich Structures and Adhesive Bonded Joints, Porto. Available from: <http://www.dogma.org.uk/vtt>.

Suquet, P., 1987. Elements of homogenization for inelastic solid mechanics. In: Sanchez-Palencia, E., Zaoui, A. (Eds.), Homogenization Techniques for Composite Media, Lecture Notes in Physics. Springer-Verlag, Berlin.

Tian, Y.S., Lu, T.J., 2005. Optimal design of compression corrugated panels. Thin Wall Strut. 43, 477–498.

Tian, J., Kim, T., Lu, T.J., Hudoson, H.P., Sypeck, D.J., Wadley, H.N.G., 2004. The effect of topology upon fluid-flow and heat-transfer within cellular copper structures. Int. J. Heat Mass Transfer 47, 3171–3186.

Vinson, J.R., 2005. Plate and Panel Structures of Isotropic, Composite and Piezoelectric Materials, including Sandwich Construction. Springer, Dordrecht, Netherlands.

Wadley, H.N.G., Fleck, N.A., Evans, A.G., 2003. Fabrication and structural performance of periodic cellular metal sandwich structures. Comput. Sci. Technol. 63, 2331–2343.

Wallach, J.C., Gibson, L.G., 2001. Mechanical behavior of a three-dimensional truss material. Int. J. Solids Strut. 38, 5165–5183.

Wicks, N., Hutchinson, J.W., 2001. Optimal truss plates. Int. J. Solids Strut. 38, 5165–5183.

Wicks, N., Hutchinson, J.W., 2003. Performance of sandwich plates with truss cores. Mech. Mater. 36, 739–751.

Ziegler, E., Accorsi, M., Bennett, M., 2004. Continuum plate model for lattice block material. Mech. Mater. 36, 753–766.